Clim. Past, 12, 455–481, 2016
www.clim-past.net/12/455/2016/
doi:10.5194/cp-12-455-2016

Climate of the Past
Open Access
EGU

A model–model and data–model comparison for the early Eocene hydrological cycle

Matthew J. Carmichael[1,2], Daniel J. Lunt[1], Matthew Huber[3], Malte Heinemann[4], Jeffrey Kiehl[5], Allegra LeGrande[6], Claire A. Loptson[1], Chris D. Roberts[7], Navjit Sagoo[1,a], Christine Shields[5], Paul J. Valdes[1], Arne Winguth[8], Cornelia Winguth[8], and Richard D. Pancost[2]

[1]BRIDGE, School of Geographical Sciences and Cabot Institute, University of Bristol, Bristol, UK
[2]Organic Geochemistry Unit, School of Chemistry and Cabot Institute, University of Bristol, Bristol, UK
[3]Climate Dynamics Prediction Laboratory, Department of Earth Sciences, The University of New Hampshire, Durham, NH, USA
[4]Institute of Geosciences, Kiel University, Kiel, Germany
[5]Climate and Global Dynamics Laboratory, UCAR/NCAR, Boulder, CO, USA
[6]NASA Goddard Institute for Space Studies, New York, NY, USA
[7]The Met Office, Exeter, UK
[8]Climate Research Group, Department of Earth and Environmental Sciences, University of Texas Arlington, Arlington, TX, USA
[a]now at: Department of Geology and Geophysics, Yale University, New Haven, CT, USA

Correspondence to: Matthew J. Carmichael (matt.carmichael@bristol.ac.uk)

Received: 19 June 2015 – Published in Clim. Past Discuss.: 17 July 2015
Revised: 3 February 2016 – Accepted: 3 February 2016 – Published: 25 February 2016

Abstract. A range of proxy observations have recently provided constraints on how Earth's hydrological cycle responded to early Eocene climatic changes. However, comparisons of proxy data to general circulation model (GCM) simulated hydrology are limited and inter-model variability remains poorly characterised. In this work, we undertake an intercomparison of GCM-derived precipitation and $P - E$ distributions within the extended EoMIP ensemble (Eocene Modelling Intercomparison Project; Lunt et al., 2012), which includes previously published early Eocene simulations performed using five GCMs differing in boundary conditions, model structure, and precipitation-relevant parameterisation schemes.

We show that an intensified hydrological cycle, manifested in enhanced global precipitation and evaporation rates, is simulated for all Eocene simulations relative to the preindustrial conditions. This is primarily due to elevated atmospheric paleo-CO_2, resulting in elevated temperatures, although the effects of differences in paleogeography and ice sheets are also important in some models. For a given CO_2 level, globally averaged precipitation rates vary widely between models, largely arising from different simulated surface air temperatures. Models with a similar global sensitivity of precipitation rate to temperature ($\mathrm{d}P/\mathrm{d}T$) display different regional precipitation responses for a given temperature change. Regions that are particularly sensitive to model choice include the South Pacific, tropical Africa, and the Peri-Tethys, which may represent targets for future proxy acquisition.

A comparison of early and middle Eocene leaf-fossil-derived precipitation estimates with the GCM output illustrates that GCMs generally underestimate precipitation rates at high latitudes, although a possible seasonal bias of the proxies cannot be excluded. Models which warm these regions, either via elevated CO_2 or by varying poorly constrained model parameter values, are most successful in simulating a match with geologic data. Further data from low-latitude regions and better constraints on early Eocene CO_2 are now required to discriminate between these model simulations given the large error bars on paleoprecipitation estimates. Given the clear differences between simulated precipitation distributions within the ensemble, our results suggest

that paleohydrological data offer an independent means by which to evaluate model skill for warm climates.

1 Introduction

Considerable uncertainty exists in understanding how the Earth's hydrological cycle will function on a future warmer-than-present planet. State-of-the-art general circulation models (GCMs) show a wide inter-model spread for future precipitation and run-off responses when prescribed with the same greenhouse gas emission trajectories (Collins et al., 2013; Knutti and Sedlácek, 2013). Remarkably few studies have investigated the hydrology of ancient greenhouse climates, but understanding how the hydrological cycle operated differently during these intervals could provide insight into the mechanisms which will govern future changes and the sensitivity of these processes (e.g. Pierrehumbert, 2002; Suarez et al., 2009; White et al., 2001). In particular, characterising the hydrological cycle simulated in GCMs using paleo-boundary conditions and comparisons to geological proxy data can contribute to developing an understanding of how well models that are used to make future predictions perform for warm climates.

Numerous proxy studies indicate that the early Eocene (56–49 Ma) was the warmest sustained interval of the Cenozoic, with evidence for substantially elevated global temperatures relative to preindustrial conditions in both marine (Zachos et al., 2008; Dunkley Jones et al., 2013; Inglis et al., 2015) and terrestrial settings (Huber and Caballero, 2011; Pancost et al., 2013). Beginning in the mid-Paleocene, a long-term warming trend resulted in bottom water temperatures increasing by about 6 °C, culminating in the sustained warmth of the Early Eocene Climatic Optimum (EECO, 53–50 Ma; Littler et al., 2014; Zachos et al., 2008). During the EECO, pollen and macrofossil evidence indicates near-tropical forest growth on Antarctica (Pross et al., 2012; Francis et al., 2008) and fossils of fauna including alligators, tapirs, and non-marine turtles occur in the Canadian Arctic (Markwick, 1998; Eberle, 2005; Eberle and Greenwood, 2012). Absolute temperatures for the Paleogene remain controversial (e.g. Taylor et al., 2013; Douglas et al., 2014; Hollis et al., 2012), but sea surface temperatures (SSTs) may have reached 26–28 °C in the southwest Pacific during this interval (TEX_{86}^{L} – tetraether index of 86 carbon atoms; Hollis et al., 2012; Bijl et al., 2009). The EECO mean annual air temperature (MAT) of Wilkes Land margin on Antarctica has been estimated to be 16 ± 5 °C (nearest living relative, NLR, based on paratropical vegetation), with summer temperatures as high as 24–27 °C, inferred from soil bacterial tetraether lipids (MBT–CBT, methylation of branched tetraethers and cyclisation of branched tetraethers; Pross et al., 2012); similar but slightly higher MATs were obtained from New Zealand (Pancost et al., 2013). Low-latitude data are scarce, but oxygen isotopes of planktic foraminifera and TEX_{86} indicate SSTs off the coast of Tanzania> 30 °C (Pearson et al., 2007; Huber, 2008). Superimposed on these longer-term trends were a series of briefer transient "hyperthermal" warmings, associated with global-scale perturbations to the carbon cycle. The most prominent of these was the Paleocene–Eocene Thermal Maximum (PETM; ∼ 56 Ma) which resulted in surface warming of between 5–9 °C above background levels (Dunkley-Jones et al., 2013; McInerney and Wing, 2011). A number of smaller-amplitude hyperthermals followed, including the Eocene Thermal Maximum 2 (ETM2), H2, I1, I2, and the K/X events (Cramer et al., 2003; Lourens et al., 2005; Stap et al., 2010), with the latter events occurring within the peak multimillion year warmth of the EECO (e.g. Kirtland-Turner et al., 2014). These later hyperthermals are also characterised by rapid warming and transient changes in the carbon cycle, although the environmental consequences are less well explored (e.g. Nicolo et al., 2007; Sluijs et al., 2009; Krishnan et al., 2014).

Determining the causes of warmth and simulating the climatic variability of this interval has been a major focus of paleoclimatic modelling. Whilst the role of paleogeographic changes throughout the Eocene is the subject of debate (e.g. Inglis et al., 2015; Bijl et al., 2013; Lunt et al., 2015), changes in greenhouse gases and carbon cycling have been widely invoked to explain both the early Eocene multimillion year warming trend and hyperthermals (e.g. Komar et al., 2013; Slotnick et al., 2012; Zachos et al., 2008). However, few proxy estimates of early Eocene atmospheric carbon dioxide exist. Paleosol geochemistry indicates that concentrations could have reached ∼ 3000 ppmv (i.e. > 10 times preindustrial CO_2; Yapp, 2004; Lowenstein and Demicco, 2006), whilst stomatal index approaches yield more modest values of 400–600 ppmv (i.e. 1.5–2 times preindustrial CO; Royer et al., 2001; Smith et al., 2010). Recent modelling indicates that terrestrial methane emissions could also have been significantly greater than modern values, representing an additional greenhouse gas forcing (Beerling et al., 2011). Considering proxy uncertainties in both age and pCO_2 calibration, these estimates represent a range of plausible atmospheric greenhouse gas concentrations with which to undertake GCM studies. However, simulating warm high-latitude and equable continental interior temperatures implied by temperature proxies has proven challenging, with models struggling to replicate the reduced Equator–pole temperature gradient implied by the proxies (Huber and Sloan, 2001; Valdes, 2011; Pagani et al., 2013, and references therein). This has resulted in the suggestion that GCMs may be missing key heat transfer processes or mechanisms for warmth (e.g. Abbot and Tziperman, 2008; Huber et al., 2004; Korty et al., 2002; Kirk-Davidoff, 2002) as well as in a re-evaluation of existing proxy data and new modelling aimed at reducing data–model anomalies (Sagoo et al., 2013; Kiehl and Shields, 2013; Loptson et al., 2014; Sluijs et al., 2006; Huber and Caballero, 2011; Lunt et al., 2012).

Table 1. Summary of model simulations in the ensemble adapted from Table 1 of Lunt et al. (2012). Additions detailing precipitation schemes are from Table 2 of Dai (2006). Some models have irregular grids in the atmosphere and/or ocean or have spectral atmospheres. The atmospheric and ocean resolution is given as $X \times Y \times Z$, where X is the effective number of grid boxes in the zonal, Y in the meridional, and Z in the vertical. e: eccentricity; o: obliquity; p: longitude of perihelion.

Model	Eocene simulation reference	Model reference	Atmosphere resolution	Ocean resolution	Paleogeography	Sim. length (years)	CO_2 levels	Orbital configuration
HadCM3L	Lunt et al. (2010)	Cox et al. (2001)	$96 \times 73 \times 19$	$96 \times 73 \times 20$	Proprietary	> 3400	× 1, 2, 4, 6	Preindustrial orbit
HadCM3L (T)	Loptson et al. (2014)						× 2, 4	
ECHAM5	Heinemann et al. (2009)	Roeckner et al. (2003)	$96 \times 48 \times 19$	$142 \times 82 \times 40$	Bice and Marotzke (2001)	2500	× 2	$e = 0.0300$; $o = 23.25$; $p = 270$
CCSM3 (W)	Winguth et al. (2010, 2012)	Collins et al. (2006); Yeager et al. (2006)	$96 \times 48 \times 26$	$100 \times 116 \times 25$	Sewall et al. (2000) with marginal sea parameterisation	1500	× 4, 8, 16	$e = 0$; $o = 23.5$
CCSM3 (H)	Liu et al. (2009); Huber and Caballero (2011)	Collins et al. (2006); Yeager et al. (2006)	$96 \times 48 \times 26$	$100 \times 122 \times 25$	Sewall et al. (2000)	1500	× 2, 4, 8, 16	Preindustrial orbit
CCSM3 (K)	Kiehl and Shields (2013)	Collins et al. (2006); Yeager et al. (2006)	$96 \times 48 \times 26$	$100 \times 116 \times 25$	As CCSM (W)	> 2000 > 3600 +	× ∼ 5 × ∼ 9	As CCSM (W)
GISS-ER	Roberts et al. (2009)	Schmidt et al. (2006)	$72 \times 45 \times 20$	$72 \times 45 \times 13$	Bice and Marotzke (2001)	2000	× ∼ 4	$e = 0.0270$; $o = 23.20$, $p = 180$
FAMOUS	Sagoo et al. (2013)	Jones et al. (2005), Smith et al. (2008).	$48 \times 37 \times 11$	$96 \times 73 \times 20$	Proprietary	> 1500	× 2	Preindustrial orbit

Model	Stratiform precipitation	Convective precipitation	Vegetation	Aerosols
HadCM3L	Large-scale precipitation is calculated based on cloud water and ice contents (similar to Smith, 1990)	Bulk mass flux scheme (Gregory and Rowntree, 1990), with improvement by Gregory et al. (1997)	Homogenous shrubland (Lunt) Dynamically evolving vegetation TRIFFID (Loptson)	As control
ECHAM5	Prognostic equations for the water phases, bulk cloud microphysics (Lohmann and Roeckner, 1996)	Bulk mass flux scheme (Tiedtke, 1989) with modifications for deep convection according to Nordeng (1994).	Homogenous woody savannah	As control
CCSM3 (W)	Prognostic condensate and precipitation parameterisation (Zhang et al., 2003)	Simplified Arakawa and Schubert (1974; cumulus ensemble) scheme developed by Zhang and McFarlane (1995)	Shellito and Sloan (2006)	As control
CCSM3 (H)			Sewall et al. (2000)	Reduced aerosol loading
CCSM3 (K)			Sewall et al. (2000)	Cloud microphysical parameters altered
GISS-ER	Prognostic stratiform cloud based on moisture convergence (Del Genio et al., 1996)	Bulk mass flux scheme by Del Genio and Yao (1993)	Sewall et al. (2000)	As control
FAMOUS	Precipitation parameterisation schemes are based on those of HadCM3L.		Homogenous shrubland	Uncertain perturbed parameters include those relating to cloud microphysical properties

Despite extensive effort to understand the causes and nature of the Eocene super-greenhouse climate state, its hydrology remains poorly characterised. Initial observations of globally widespread Eocene laterites and coals (Frakes, 1979; Sloan et al., 1992) and of enhanced sedimentation rates and elevated kaolinite in the clay fraction of many coastal sections (Bolle et al., 2000; Bolle and Adatte, 2001; John et al., 2012; Robert and Kennett, 1994; Nicolo et al., 2007) suggested that early Eocene terrestrial environments were characterised by globally enhanced precipitation and run-off relative to today. Diverse geochemical proxies are now providing a more nuanced interpretation of how the spatial organisation of the Eocene hydrological cycle differed from that of the present day. This is particularly the case for the PETM. In the Arctic, the hydrogen isotopic composition of putative leaf-wax compounds became enriched by $\sim 55\,‰$ δD at the PETM, thought to reflect increased export of moisture from low latitudes (Pagani et al., 2006). Enrichment of δD in leaf waxes from tropical Tanzania, coincident with elevated concentrations of terrestrial biomarkers and sedimentation rates, has been interpreted as indicating a shift to a more arid climate with seasonally heavy rainfall (Handley et al., 2008, 2012). Whether these changes are typical of the low latitudes or are highly localised responses remains to be determined. Elsewhere, conflicting evidence for regional hydrological changes exists: an increased PETM offset in the magnitude of the carbon isotope excursion (CIE) between marine and terrestrially derived carbonates, including from Wyoming, has been suggested to reflect increases in humidity and soil moisture of the order of 20–25 % (Bowen et al., 2004). Other studies utilising leaf physiognomy and paleosols suggest that the North American continental interior became drier at the onset of the PETM or alternated between wet and dry phases (Kraus et al., 2013; Smith et al., 2007; Wing et al., 2005).

These proxies collectively indicate an early Eocene hydrological cycle different to that of the present day, but only limited proxy–model comparisons have been made (Pagani et al., 2006; Speelman et al., 2010; Winguth et al., 2010). Such comparisons will be valuable for a better understanding of the climate of warm time intervals but also offer an alternative to temperature by which to evaluate GCM performance and/or constrain boundary conditions. Some analysis of model precipitation and $P-$ sensitivity to imposed CO_2 (Winguth et al., 2010), paleogeography (e.g. Roberts et al., 2009), and parametric uncertainty (Sagoo et al., 2013; Kiehl and Shields, 2013) has been undertaken, but the range of hydrological behaviour simulated within different models has not yet been assessed. Broadly, GCMs indicate that future warmth will be associated with an exacerbated $P - E$ distribution, as increased water vapour transport occurs from moisture divergence zones into convergence zones (Held and Soden, 2006; Chou and Neelin, 2004). An intensified hydrological cycle, associated with increased meridional transport of water vapour is therefore consistent with regions of both wetting and drying, although this thermodynamic response may be complicated by dynamical shifts in atmospheric circulation (e.g. Chou et al., 2009; Bony et al., 2013; Chadwick et al., 2012). However, these hypotheses remain largely untested on ancient climate states. Lunt et al. (2012) undertook a model intercomparison of early Eocene warmth, EoMIP, based on an ensemble of 12 Eocene simulations undertaken in four fully coupled atmosphere–ocean climate models, a summary of which is given in Table 1. This demonstrated differences in global surface air temperature of up to 9 °C for a single imposed CO_2 and differing regions of CO_2-induced warming, but the implications for the hydrological cycle have not been considered.

This study addresses three main questions. (1) How do globally averaged GCM precipitation rates for the Eocene

compare to preindustrial simulations and vary between models in the EoMIP ensemble? (2) How consistently do the EoMIP GCMs simulate regional precipitation and $P-E$ distributions? (3) Do differences between models affect the degree of match with existing proxy estimates for mean annual precipitation?

2 Model descriptions

The EoMIP approach of Lunt et al. (2012) is distinct from formal model intercomparison projects which utilise a common experimental design (e.g. PMIP3, Paleoclimate Modelling Intercomparison Project Phase III, Taylor et al., 2012; CMIP5, Coupled Model Intercomparison Project, Phase 5; Braconnot et al., 2012). Instead, the EoMIP models differ in their boundary conditions and span a plausible early Eocene CO_2 range, utilise different paleogeographic reconstructions, and specify different vegetation distributions. This is in addition to internal differences in model structure and physics, including precipitation-relevant parameterisations such as those relating to convection and cloud microstructure. Whilst this may hinder the identification of reasons for inter-model differences, the ensemble spans more fully the uncertainty in boundary conditions, which is appropriate for deep-time climates such as the early Eocene.

The ensemble, summarised in Table 1, includes a range of published simulations of the early Eocene carried out with fully dynamic atmosphere–ocean GCMs. We extend the EoMIP ensemble as originally described by Lunt et al. (2012) to include simulations published by Sagoo et al. (2013), Kiehl and Shields (2013), and Loptson et al. (2014). A brief description of each model and the corresponding simulation is given below. Each model produces large-scale (stratiform) and convective precipitation separately, also summarised in Table 1. Greenhouse gases other than CO_2 are only varied in some of the simulations and are held at preindustrial levels in a number of the models; we have therefore estimated the forcing in terms of net CO_2 equivalent, as detailed below. We refer to the simulations throughout this paper in terms of their atmospheric CO_2 level relative to preindustrial conditions (i.e. an Eocene simulation with an atmospheric CO_2 concentration twice that of preindustrial conditions is referred to as "x2" and one with a concentration four times that value is referred to as "x4").

2.1 HadCM3L

HadCM3L (Hadley Centre Coupled Model, Version 3L) is a version of the GCM developed by the UK Met Office (Cox et al., 2000). Eocene simulations performed at x2, x4, and x6 preindustrial concentrations of atmospheric CO_2 were presented by Lunt et al. (2010) in their study of the role of ocean circulation as a possible PETM trigger via methane hydrate destabilisation. In these simulations, models were integrated for more than 3400 years to allow intermediate-depth ocean temperatures to equilibrate. Both the atmosphere and ocean are discretised on a 3.75° longitude × 2.5° latitude grid, with 19 vertical levels in the atmosphere and 20 in the ocean. Vegetation is set to a fixed globally homogenous shrubland.

The effect of using an interactive vegetation model, TRIFFID (Top–down Representation of Interactive Foliage and Flora Including Dynamics; Cox, 2001), on temperature proxy–model anomalies was considered by Loptson et al. (2014), who performed simulations at x2 and x4 preindustrial CO_2, continuations of those of Lunt et al. (2010). Within each grid cell, TRIFFID simulates the fractional coverage of five plant functional types, which in turn influences climate via feedbacks including albedo, evapotranspiration rate, and carbon cycling (Cox et al., 2001). This study indicated that for a given prescribed CO_2, the inclusion of dynamic vegetation acts to warm global climate via albedo and water vapour feedbacks. We refer to these simulations as HadCM3L (T). The effect of dynamic vegetation on precipitation distributions and global precipitation rate was additionally briefly considered, but comparisons to precipitation proxy data or to other models have not been undertaken.

2.2 FAMOUS

FAMOUS (Fast Met Office/UK Universities Simulator) is an alternative version of the UK Met Office's GCM, adopting the same climate parameterisations as HadCM3L but solved at a reduced spatial and temporal resolution in the atmosphere (Jones et al., 2005; Smith et al., 2008). Atmospheric resolution is 7.5° longitude × 5° latitude, with 11 levels in the vertical, whilst the ocean resolution matches that of HadCM3L. Both modules operate at an hourly time step. Because of its reduced resolution, FAMOUS has been used for transient simulations with long run times and in perturbed parameter ensembles where a large number of simulations are required (Smith and Gregory, 2012; Williams et al., 2013). Sagoo et al. (2013) used FAMOUS to study the effect of parametric uncertainty on early Eocene temperature distributions by varying 10 climatic parameters which are typically poorly constrained in climate models. Their results demonstrated that a globally warm climate with a reduced Equator-to-pole temperature gradient can be achieved at x2 preindustrial CO_2 level. Of the 17 successful simulations which ran to completion, our focus is on E16 and E17, the simulations which have the shallowest Equator-to-pole temperature gradient and which show the optimal match to marine and terrestrial temperature proxy data. At the ocean grid resolution, the paleogeography matches that of Lunt et al. (2010). Vegetation is set to a fixed homogenous shrubland. All simulations were run for a minimum of 8000 model years and full details of the perturbed parameters are provided in Sagoo et al. (2013). Sagoo et al. show DJF and JJA precipitation distributions for their globally warmest and coolest simulations, but comparisons to other models or to proxy data have not been made.

2.3 CCSM3

We utilise three sets of simulations performed with CCSM3 (Community Climate System Model, Version 3), a GCM developed by the US National Centre for Atmospheric Research in collaboration with the university community (Collins et al., 2006). The first set was initially used by Liu et al. (2009) in their study of Eocene–Oligocene sea surface temperatures and subsequently compared to terrestrial proxy data in a study of the early Eocene climate equability problem by Huber and Caballero (2011). These simulations are configured with atmospheric CO_2 at x2, x4, x8, and x16 preindustrial. Models were integrated for between 2000 and 5000 years until the sea surface temperature was in equilibrium. The atmosphere is resolved on a 3.75° longitude by $\sim$3.75° latitude (T31) grid with 26 levels in the vertical, and the ocean is resolved on an irregularly spaced dipole grid. The prescribed land surface cover follows the reconstructed vegetation distribution utilised in Sewall et al. (2000). Following the approach of Lunt et al. (2012), we refer to these simulations as CCSM3 (H).

The second set of simulations, which we refer to as CCSM3 (W), was described by Winguth et al. (2010) and Shellito et al. (2009) and conducted at x4, x8, and x16 preindustrial CO_2. Relative to the CCSM3 (H) simulations, these simulations utilised a solar constant reduced by 0.44 %, adopted an updated vegetation distribution (Shellito and Sloan, 2006), and utilised a marginal sea parameterisation, resulting in paleogeographic differences, particularly in polar regions. However, the major difference between the simulations is that the CCSM3 (W) simulations utilise a modern-day aerosol distribution, whereas CCSM3 (H) adopts a reduced loading for the early Eocene based on a hypothesised lower early Eocene ocean productivity (Kump and Pollard, 2008; Winguth et al., 2012).

The third set of simulations, CCSM3 (K), is described in Kiehl and Shields (2013). This study investigated the sensitivity of Eocene climatology to the parameterisation of aerosol and cloud effects, specifically by altering cloud microphysical parameters including cloud drop number and effective cloud drop radii. Modern-day values from pristine regions are applied homogenously across land and ocean. Simulations were performed at two greenhouse gas concentrations corresponding to possible pre- and trans-PETM atmospheric compositions which are equivalent to about x5 and about x9 preindustrial CO_2 levels respectively. Paleogeography and vegetation distribution are the same as those used in CCSM3 (W), and the solar constant is reduced by 0.487 % relative to the preindustrial value. Changes in precipitation distribution between high- and low-CO_2 simulations have previously been shown for the CCSM3 (W) and CCSM3 (K) simulations (Winguth et al., 2010; Kiehl and Shields, 2013), but how robust these Eocene distributions are to GCM choice remains unknown.

2.4 ECHAM5/MPI-OM

The ECHAM5/MPI-OM (European Centre Hamburg Model, Version 5, and Max Planck Institute Ocean Model) model is the GCM of the Max Planck Institute for Meteorology (Roeckner et al., 2003), used by Heinemann et al. (2009) in their study of reasons for early Eocene warmth. The simulation was performed at x2 preindustrial CO_2, using the paleogeography of Bice and Marotzke (2001) and a globally homogenous vegetation cover, with lower albedo but larger leaf area and forest fraction than preindustrial, equivalent to a modern-day woody savannah. Atmosphere components are resolved on a Gaussian grid, with a spacing of 3.75° longitude and approximately 3.75° latitude. Relative to the preindustrial simulation, methane is increased from 65 to 80 ppb and nitrous oxide from 270 to 288 ppb for the Eocene, but these are negligible relative to change in radiative forcing associated with a doubling of preindustrial CO_2. Latitudinal precipitation distributions in the simulation relative to the preindustrial conditions were considered by Heinemann et al. (2009) and elevated convective precipitation at high latitudes was suggested to be consistent with convective clouds as a high-latitude warming mechanism (Abbot and Tziperman, 2008).

2.5 GISS-ER

The E-R version of the Goddard Institute for Space Studies model (GISS-ER; Schmidt et al., 2006) was utilised by Roberts et al. (2009) in their study of the impact of Arctic paleogeography on high-latitude early Eocene sea surface temperature and salinity. Here, we include the simulation with the open Arctic paleogeography of Bice and Marotzke (2001) which is also utilised in the ECHAM5 simulation. The simulation was performed with CO_2 at x4 preindustrial levels and CH_4 at x7 preindustrial levels, equivalent to a total Eocene greenhouse gas forcing of about x4.3 preindustrial CO_2. The atmospheric component of GISS-ER has a grid resolution of 4° latitude by 5° longitude with 20 levels in the vertical; the ocean model is of the same horizontal resolution but with 13 levels. Vegetation is prescribed as in Sewall et al. (2000). The hydrological cycle is shown to be intensified for the Paleogene simulation, with elevated global precipitation and evaporation rates, but spatial precipitation distributions were not studied.

3 Results

3.1 Preindustrial simulations

The simulation of precipitation is a particular challenge for GCMs given the range of spatial and temporal scales on which precipitation-producing processes occur, compared to a typical model grid and time step (e.g. Knutti and Sedlacek, 2013; Hagemann et al., 2006). Model resolution and the parameterisation schemes which account for sub-grid-scale

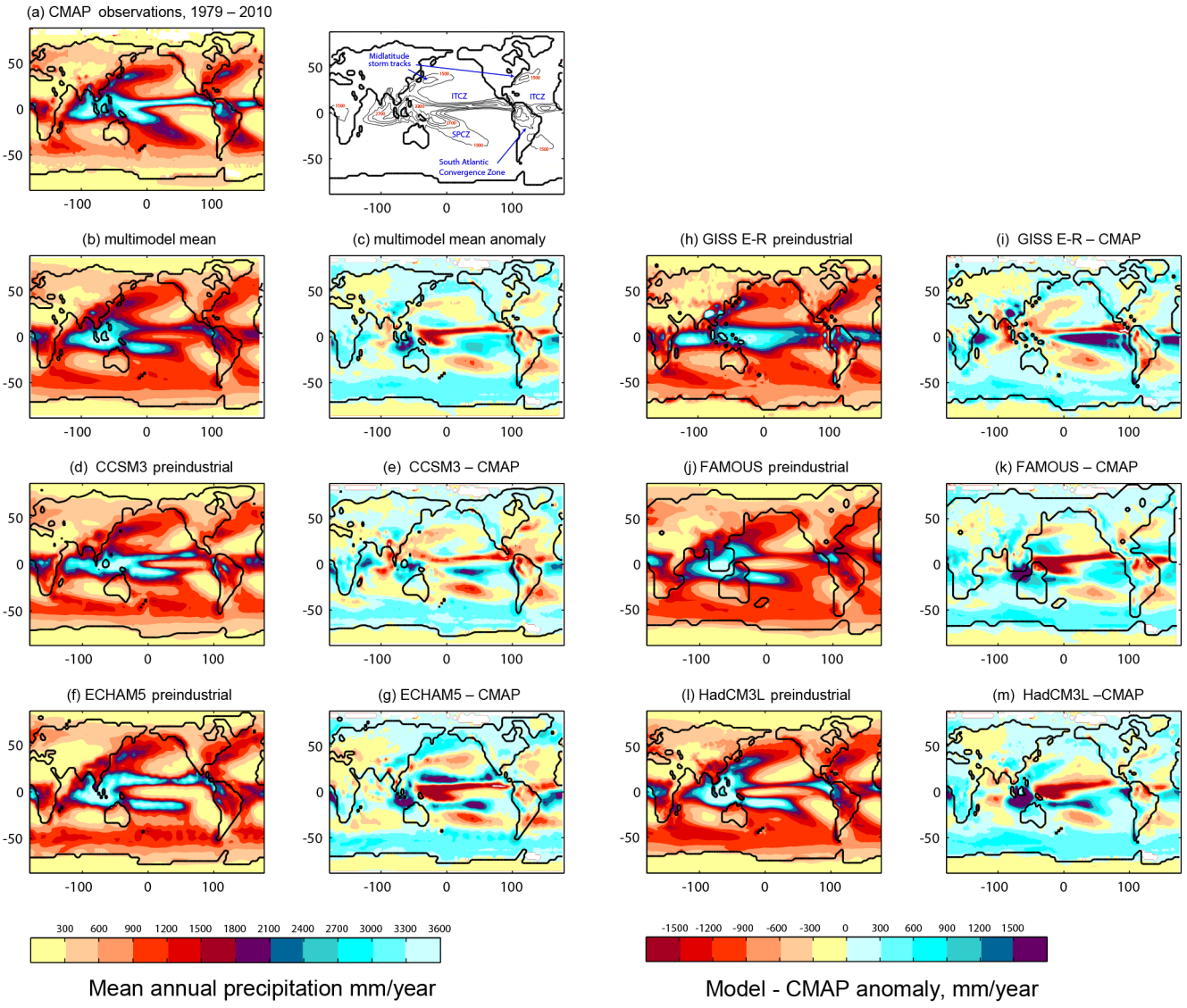

Figure 1. Preindustrial precipitation distributions as simulated in the EoMIP models (modern paleogeography). Panels **(a, b, d, f, h, j)**, and **(l)** show mean annual precipitation (MAP; left colour bar), and panels **(c, e, g, i, k)**, and **(m)** show anomalies relative to CMAP observations (1979–2010) calculated as model minus observations (right colour bar). The inset to the right of **(a)** indicates the principal features of the CMAP precipitation distribution, as discussed in the text.

precipitation, in addition to temperature distributions, differ between the GCMs in the ensemble (Table 1). We initially summarise model skill in simulating preindustrial mean annual precipitation (MAP) to provide context for our Eocene model intercomparison and to identify which, if any, precipitation structures are unique to the Eocene and which are more fundamentally related to errors particular to a given GCM.

Figure 1 shows preindustrial MAP distributions for each GCM in the EoMIP ensemble and anomalies for each preindustrial simulation relative to CMAP observations (Centre for Climate Prediction, Merged Analysis of Precipitation), which incorporates both satellite and gauge data (Yin et al., 2004; Gruber et al., 2000). The following observations can be made.

i. All of the EoMIP GCMs simulate the principal features of the observed preindustrial MAP distribution, although errors occur in their position and strength. The Inter-tropical Convergence Zone (ITCZ), North Atlantic and North Pacific storm tracks, and subtropical precipitation minima over eastern ocean basins are identifiable for each simulation, but differences are evident between the models. Some biases are common to a number of the models, in particular those relating to the ITCZ and tropical precipitation. HadCM3L, FAMOUS,

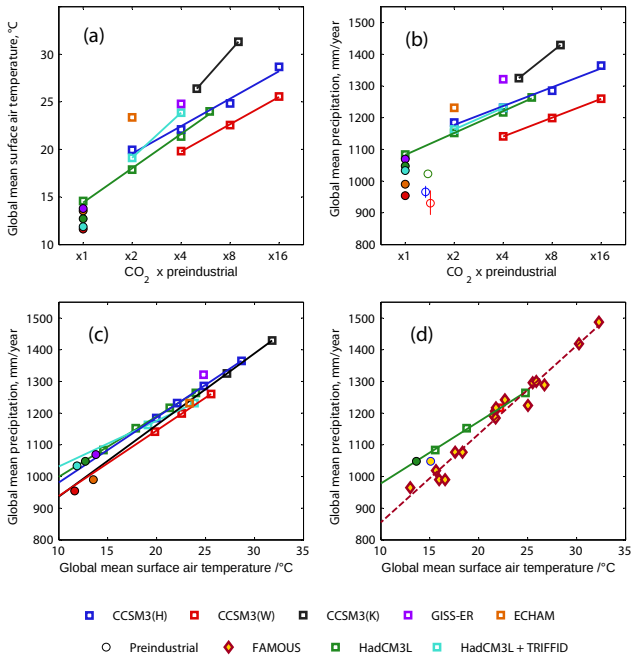

Figure 2. Global sensitivity of the Eocene hydrological cycle in the EoMIP simulations. Global mean surface air temperature relative to model CO_2 **(a)**, global mean precipitation rate relative to model CO_2 **(b)**, and global mean surface air temperature **(c)**; note the logarithmic scale on the horizontal axis in **(a, b)**. Preindustrial simulations and Eocene simulations are shown as circles and squares respectively. The CCSM3 simulations share a preindustrial simulation, shown in red. Open circle symbols in **(b)** show modern-day estimates of global precipitation rate calculated based on CMAP data (red), GPCP data (Global Precipitation Climatology Project; Adler et al. 2003; blue), and Legates and Willmott (1990) climatology (green). Also shown is the sensitivity of the hydrological cycle to global mean surface air temperature in the 17 successful simulations of Sagoo et al. (2013) using FAMOUS (**d**; diamonds), with HadCM3L simulations (blue; Lunt et al., 2010) shown for comparison. All best-fit lines are based on Eocene simulations only.

ECHAM5, and CCSM3 all simulate the ITCZ mean annual location north of the Equator, but the South Pacific Convergence Zone (SPCZ) generally extends too far east within the Pacific and is too zonal, with precipitation equalling that to the north of the Equator to produce a "double-ITCZ" – a common bias in GCMs (Dai, 2006; Lin et al., 2007; Brown et al., 2011). The localised rain belt minimum is a result of the Pacific cold tongue, not present in GISS-ER, which instead simulates a single convergence zone with high mean annual precipitation across the tropics. Other biases which appear common across the ensemble include too little precipitation over the Amazon (Yin et al., 2013; Joetzjer et al., 2013), over-precipitation in the Southern Ocean (Randall et al., 2007, and references therein), and biases in the position of rainfall maxima in the Indo-Pacific (e.g. Liu et al., 2014).

ii. Errors over the continents are smaller than those over the oceans. Absolute errors in MAP are largest over the high-precipitation tropical and subtropical oceans and frequently exceed 150 cm yr^{-1} in the case of ITCZ and SPCZ offsets. Over the continents, anomalies are generally no greater than 60 cm yr^{-1}, and more than 80 % of the multimodel mean terrestrial surface has an anomaly less than 30 cm yr^{-1}. In low-precipitation regions, these errors still result in significant percentage errors (Fig. S1 in the Supplement).

iii. Models show regional differences in precipitation skill. Figure 1 demonstrates that some precipitation biases are individual to particular GCMs. Whilst these are most noticeable over the high-precipitation tropical and subtropical oceans, such as offsets in the location of maximum precipitation intensity or strength of storm tracks, relative differences within low-precipitation continental regions can also be considerable (Mehran et al., 2014; Phillips and Gleckler, 2006). This is particularly the case for the Sahel region of northern Africa and the Antarctic continental interior (Fig. S2). We hypothesise that GCMs applied to the study of paleoclimates are also likely to show significant regional differences in their precipitation distribution, underlining the importance of model intercomparison. Given that all of the models simulate the principal features of MAP distribution, we carry all forward to our Eocene analysis. However, it is important to recognise that significant model biases in simulating precipitation distribution exist, even where boundary conditions are well constrained.

3.2 Sensitivity of the global Eocene hydrological cycle to greenhouse gas forcing

The EoMIP model simulations were configured with a range of plausible early Eocene and PETM atmospheric CO_2 levels, yielding a range of global mean surface air temperatures (Lunt et al., 2012). It is therefore possible to evaluate how consistently precipitation rates are simulated across the GCMs (i) for a given CO_2 level, (ii) for a given global mean temperature or, in the case of those models for which multiple simulations have been performed, (iii) for a given CO_2 change, and (iv) for a given global mean temperature change. Closure of the GCM global hydrological budget requires that total annual precipitation and evaporation are equal, providing there is no net change in water storage; the imbalances, summarised in Table S1 in the Supplement are < 0.01 mm day^{-1} equivalent. The mean annual global precipitation rate therefore provides a zero-order indication of the intensity of the global hydrological cycle. Precipitation rates calculated from three modern observational data sets are shown in Fig. 2b (open circles); model-estimated rates

Table 2. Summary of relationships between global surface air temperature and precipitation rate. [1] T: SAT (°C); P: global precipitation (mm yr^{-1}). [2] Precipitation sensitivity is calculated over the range of 15–30 °C.

Model simulations	$P-T$ regression[1]	% increase P per °C warming over range[2]
HadCM3L	$P=19.51\,T+782.89$	1.81
HadCM3L (T)	$P=14.33\,T+874.01$	1.32
CCSM3 (H)	$P=21.38\,T+738.22$	2.02
CCSM3 (K)	$P=22.61\,T+710.60$	2.15
CCSM3 (W)	$P=21.46\,T+696.28$	2.11
FAMOUS	$P=27.86\,T+576.22$	2.80

derived from preindustrial simulations (filled circles) are in relatively good agreement with observational data, providing confidence in this measure.

All of the EoMIP models exhibit a more active hydrological cycle for the Eocene (Fig. 2b; squares) compared to that simulated in the corresponding preindustrial simulations (Fig. 2b; circles). For a given CO_2, the models vary in the intensity of the hydrological cycle they simulate; for example, ECHAM5 has a global precipitation rate at x2 preindustrial CO_2 comparable to that of CCSM3 (W) at about x12 CO_2. In the remainder of this section, we discuss reasons for these differences, which can be attributed to (i) differences in Eocene boundary conditions, including CO_2, (ii) variation of poorly constrained parameter values, and (iii) more fundamental differences in the ways in which the models simulate hydrology.

The GCMs within the EoMIP ensemble differ in their global mean temperature for a given CO_2 (e.g. Lunt et al., 2012; Fig. 2a). Consequently, the global precipitation rate for each ensemble member is shown in Fig. 2c relative to its globally averaged surface air temperature. This demonstrates that much of the variation between models in precipitation rate arises from these temperature differences. For example, the elevated precipitation rate in the x2 CO_2 ECHAM5 is explained by this model's warmth, being globally > 5 °C warmer than HadCM3L at the same CO_2. Similarly, the enhanced precipitation rate in the CCSM3 (K) simulations at both about 5 times CO_2 and about 9 times CO_2 relative to those simulated in CCSM3 (H) and CCSM3 (W) are attributable to warmer surface temperatures in CCSM3 (K), resulting from alterations to cloud condensation nuclei (CNN) parameters, with a reduction in low-level cloud acting to increase short-wave heating at the surface (Kiehl and Shields, 2013). The reduced aerosol loading in CCSM3 (H) results in surface warming relative to CCSM3 (W) (Fig. 2a), which explains much of the 7–8 % increase in strength of the hydrological cycle across the CO_2 range studied. There are effects beyond those induced by surface temperature, however. For example, for a given surface air temperature, the global precipitation rate is consistently weaker in CCSM (W) relative to CCSM (H) (Fig. 2c), possibly a result of modified aerosol–cloud interactions due to the changes in prescribed aerosols in CCSM (H).

The degree to which the global hydrological cycle will intensify with future global warming has received much attention (e.g. Allen and Ingram, 2002; Held and Soden, 2006; Trenberth, 2011). Held and Soden (2006) show a ∼ 2% increase in global precipitation per degree of warming for AR4 GCMs forced with the A1B emissions scenario but with notable inter-model variability. For those simulations with multiple CO_2 forcing, it is possible to estimate how this sensitivity varies for the Eocene. We show the $\mathrm{d}P/\mathrm{d}T$ relationships for each model as well as the increase in percentage of precipitation for a 1 °C temperature increase over the range of 15–30 °C (Table 2). Both CCSM3 and HadCM3L appear to be broadly comparable at ∼ 1.8–2.1% increase in the intensity of the hydrological cycle for each degree of warming, consistent with the future-climate simulations.

Some variation in the intensity of the hydrological cycle simulated by the EoMIP models may be expected to occur independently of global mean surface air temperature. For preindustrial conditions, boundary conditions are largely constant across the simulations (atmospheric composition, continental positions, orography, and ice sheet distribution), yet the simulations show a spread of ∼ 0.30 mm day^{-1}, which exceeds the precipitation increase for a doubling of CO_2 from x2 to x4 preindustrial levels in both CCSM3 (H) (0.13 mm day^{-1}) and HadCM3L (0.18 mm day^{-1}). Differences in global precipitation rate between the preindustrial simulations are not explained by differences in temperature (Fig. 2b) but may relate to more fundamental differences in model physics, particularly between HadCM3L and CCSM3 (W) given that a more active hydrological cycle is consistently simulated in HadCM3L for both the Eocene and preindustrial conditions. Further simulations using equivalent precipitation parameterisation schemes for large-scale and convective precipitation would be required to fully evaluate this hypothesis.

For both x2 and x4 CO_2 simulations, the HadCM3L simulations that include the TRIFFID dynamic vegetation model have a near-identical precipitation rate to those without (Fig. 2b). However, the x4 CO_2 simulation with dynamic vegetation is substantially warmer than the x4 CO_2 simulation with fixed homogenous shrubland. The inclusion of the dynamic vegetation model acts to warm the surface climate as described in Loptson et al. (2014), but this does not yield an associated increase in precipitation. Relative to the fixed shrubland simulations, the TRIFFID simulations show a reduction in continental evapotranspiration in response to a doubling of CO_2, which results in diminished moisture availability over the tropical landmass, for a given temperature (Fig. S3). The TRIFFID simulations therefore exhibit a reduced hydrological sensitivity of an only ∼ 1.3 % increase in precipitation per degree of warming ($\mathrm{d}P/\mathrm{d}T$) compared with ∼ 1.8 % for the non-TRIFFID simulations.

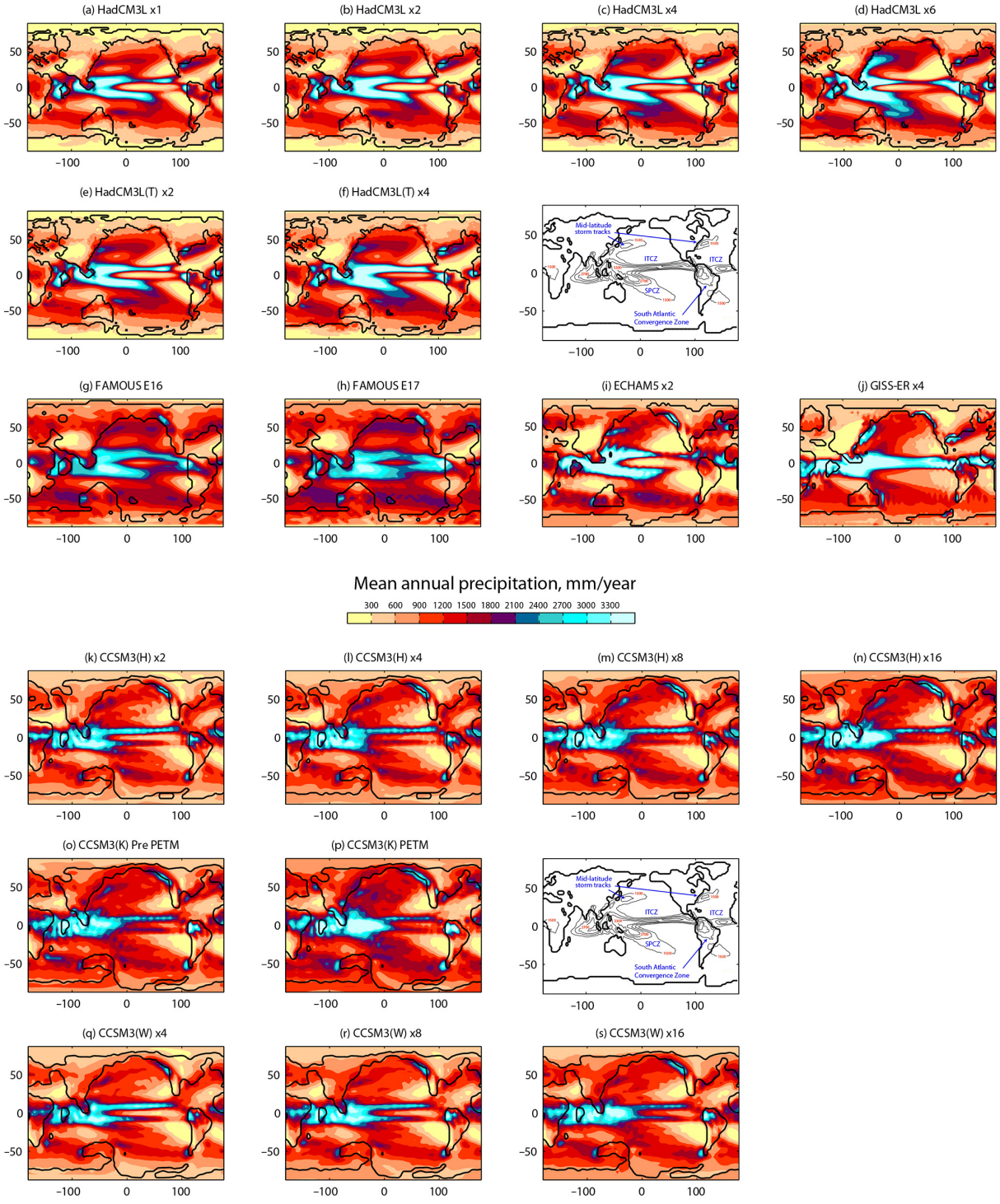

Figure 3. Mean annual precipitation distributions for each member of the EoMIP ensemble in millimetre per year (early Eocene paleogeography; ∼ 55 Ma). CO_2 for each model simulation is shown above each plot. The FAMOUS simulations are both at x2 CO_2.

In the FAMOUS simulations undertaken by Sagoo et al. (2013; Fig. 2d), all simulations are performed at x2 CO_2, but global temperatures range between 12.3 and 31.8 °C on account of simultaneous variation of 10 uncertain parameter values, some of which directly influence cloud formation and precipitation. Within these simulations there is also a linear relationship between surface air temperature and global precipitation ($R^2 = 0.965$; $n = 17$), suggesting that the global intensity of the hydrological cycle remains primarily coupled to global temperature, despite greater scatter around the dP/dT relationship. Despite this, the overall dP/dT relationship in FAMOUS is higher than that of HadCM3L and HadCM3L (T), with a ∼ 2.8 % increase in precipitation for each degree of warming (Table 2).

In HadCM3L, the Eocene simulation at x1 CO_2 and preindustrial simulations have similar global precipitation rates (Fig. 2a), implying that Eocene boundary conditions other than CO_2 do not exert a major influence on the intensity of the hydrological cycle, raising the global precipitation rate by only ∼ 0.10 mm day^{-1}. Moreover, even this small increase is consistent with and likely driven by a small increase in global surface air temperature. Furthermore, the preindustrial simulations for both CCSM3 and HadCM3L lie on, or close to, the Eocene-derived dP/dT lines (Fig. 2c), suggesting that globally, the precipitation rate for a given temperature is not increased or decreased for the Eocene, despite differences in low-latitude land–sea distribution, ocean gateways, and a lack of Eocene ice sheets. Intriguingly, extrapolating the dP/dCO_2 relationship backwards to x1 CO_2 for CCSM (W) would require an Eocene precipitation rate ∼ 7 % above that of the preindustrial rate. This suggests a more substantial effect of Eocene boundary conditions on elevating absolute precipitation rates for CCSM3 (W) than that seen in HadCM3L, but one that is still operating via temperature effects. GISS-ER has a marginally more vigorous hydrological cycle than the other models for a given global temperature. Roberts et al. (2009) show that the global precipitation rate in a preindustrial simulation with x4 CO_2 in GISS-ER is ∼ 4 % greater than that of preindustrial conditions, whereas the Paleogene simulation has a precipitation rate ∼ 23 % above that of the preindustrial conditions. Therefore, non-greenhouse gas Paleogene boundary conditions are crucial in elevating the precipitation rate in this model, in contrast to HadCM3L. However, this also appears to be mediated by temperature effects, given that the Eocene simulations of Roberts et al. (2009) are also substantially warmer than preindustrial geography simulations x4 CO_2 greenhouse gas concentrations.

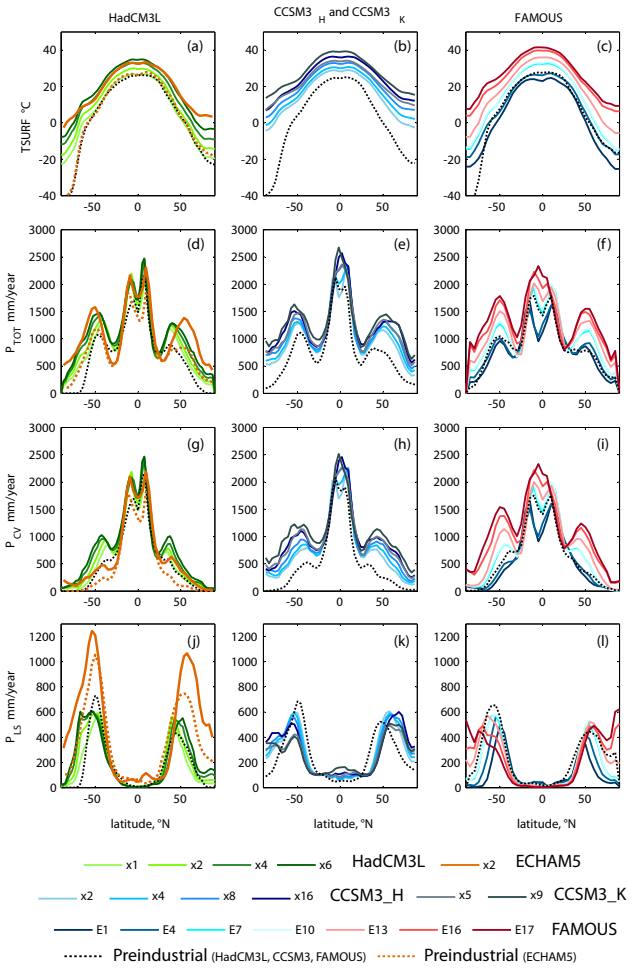

Figure 4. Latitudinal temperature and precipitation distributions in the HadCM3L and ECHAM5 (left), CCSM3 (H) and CCSM3 (K) (centre), and FAMOUS (right) members of the EoMIP ensemble. Panels **(a–c)** show mean surface air temperature, **(d–f)** total precipitation rate, **(g–i)** convective precipitation, and **(j–l)** large-scale precipitation. The HadCM3L, ECHAM5, and CCSM3 atmospheric CO_2 levels are shown in the key. All FAMOUS simulations are x2 CO_2 but differ in value for 10 uncertain parameters (Sect. 2). Simulation names E1–E17 shown in the legend correspond to those given by Sagoo et al. (2013). Black dotted lines show output from preindustrial simulations, with the exception of ECHAM5, shown in orange.

3.3 Variability in mean annual precipitation (MAP) distribution

3.3.1 Spatial distribution of MAP

Figure 3 shows MAP distributions for each EoMIP simulation. Eocene distributions are relatively similar to those for preindustrial conditions (Fig. 1), with clearly recognisable ITCZ and SPCZ structures, and subtropical precipitation minima, the distributions of which appear to be long-standing characteristics of Cenozoic precipitation. Relative

to preindustrial simulations, the Eocene distributions exhibit increased precipitation at high latitudes as a consequence of elevated temperatures in these regions. In CCSM in particular, the Eocene is characterised by a more globally equable precipitation rate: the expansion of zones of highest precipitation in the Eocene relative to preindustrial conditions is muted compared with a more extensive loss of low-precipitation regions. Additional support for this is provided by a comparison of mean precipitation rates for land and ocean (Table S2). The preindustrial ratio of land : ocean precipitation is maintained in the Eocene HadCM3L and ECHAM5 simulations, whereas in CCSM, precipitation rates over land and ocean are typically equal. The effects of differences in simulated surface air temperatures between models within the ensemble are also evident: for a given global surface temperature, HadCM3L maintains cooler poles than CCSM3 and ECHAM5 (Sect. 3.3.2), and regions with MAP $< 300\,\mathrm{cm\,yr^{-1}}$ persist in the Arctic and Antarctic, even x4 CO_2.

Modelled Eocene MAP features are frequently traceable to those identified in preindustrial simulations (Sect. 3.1), including the single tropical convergence zone in the GISS-ER simulation at x4 CO_2 and the double ITCZ in a number of the models. Elsewhere, the Eocene precipitation distributions diverge from those of the preindustrial simulations and may be related to specific Eocene paleogeography, elevated CO_2, or other boundary conditions. In HadCM3L, there is a clear trend towards a more south-easterly trending SPCZ in the higher-CO_2 simulations, which is not replicated in the warm simulations of the sister model FAMOUS. The SPCZ in CCSM3 is also far weaker in the Eocene simulations, compared to preindustrial simulations. The mechanisms which control the SPCZ in the modern day, particularly its northwest–southeast orientation, are only partially understood, with zonal SST gradients, the intensity of trade winds, and the height of the Andes all suggested to be important influences (Matthews, 2012; Cai et al., 2012). In the EoMIP simulations, CCSM3 shows much slacker surface winds at the Equator with reduced low-level convergence, whilst HadCM3L maintains stronger convergence of south-easterly trade winds with north-easterlies originating from the Pacific subtropical high (Fig. S4). Despite similar preindustrial precipitation distributions over tropical Africa, CCSM3 and HadCM3L strongly diverge in the Eocene, with CCSM3 showing far more intense equatorial precipitation. In CCSM3, evaporation is consistently less than the precipitation rate, which likely results in the recharge of soil moisture throughout the year and an availability of moisture for convective precipitation. The FAMOUS simulations E16 and E17 represent two realisations of very warm climates with a reduced Equator–pole temperature gradient; in these simulations significant increases in midlatitude precipitation are particularly accentuated over the Pacific Ocean. Increases in convection in the subtropics and midlatitudes are sufficient to eliminate the precipitation minima seen in other models at these latitudes.

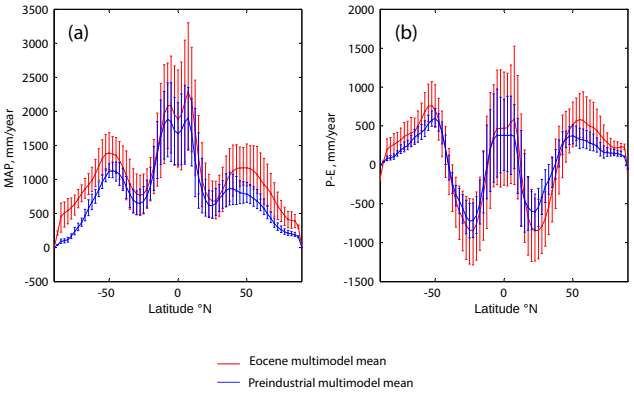

Figure 5. Multimodel mean annual precipitation **(a)** and mean annual precipitation–evaporation ($P - E$) rate **(b)** for Eocene (red) and preindustrial (blue) boundary conditions. For the Eocene multimodel mean, simulations have a global mean precipitation rate of $3.40 \pm 0.02\,\mathrm{mm\,day^{-1}}$ (Table S1); these are HadCM3L (x4), HadCM3L (T) (x4), ECHAM5 (x2), CCSM3 (H) (x4), and a linearly interpolated distribution between the x4 and x8 CO_2 CCSM3 (W) simulations. Error bars represent the range in values across simulations.

For a given CO_2, differing boundary conditions, parameterisation schemes, and simulated model air temperatures prevent direct assessment of whether Eocene regional precipitation distributions are robust across different GCMss. Model simulations have a substantially different amount of water vapour in the atmosphere and differing global precipitation rates and it is not meaningful to average these simulations. Instead, we show a multimodel mean in Fig. 5 for simulations with a common global precipitation rate to provide an assessment of regional variability between model simulations with the same global strength hydrological cycle. Elevated high-latitude precipitation for the early Eocene relative to preindustrial conditions is robust between GCMs, although absolute values remain variable between models, particularly in the Southern Hemisphere, likely due to differing Antarctic orography. Differences between models in the midlatitudes are smaller, resulting in some confidence that the secondary precipitation maxima were polewards of their preindustrial location during the Eocene. Equatorial precipitation remains highly variable between models but is accentuated relative to preindustrial conditions.

3.3.2 Controls on precipitation distribution

Precipitation rates for each simulation are summarised in Table S2, including separate rates calculated over land and ocean surfaces and rates deconvolved into those arising from convective and large-scale contributions. These data show that elevated precipitation rates in the high-CO_2 Eocene simulations are largely the result of increased convection, al-

though in the ECHAM5 model a greater percentage of precipitation is generated by large-scale mechanisms in both the Eocene and preindustrial simulation. Figure 4 shows how convective and large-scale precipitation rates vary with latitude for a selection of the EoMIP simulations. This reveals differences between models in the mechanisms responsible for precipitation distributions which can be related to surface air temperature distributions. In the HadCM3L simulations, the midlatitude maxima in both large-scale and convective precipitation advance polewards with increasing CO_2, with precipitation increases over the high northern latitudes driven almost exclusively by enhanced large-scale precipitation. CCSM3 has substantially warmer poles, which results in much enhanced high-latitude large-scale precipitation relative to HadCM3L, although large-scale latitudinal contributions differ somewhat for preindustrial simulations at both low and high latitudes. In CCSM3 (K), the warmest CCSM3 simulations, polar temperatures are elevated compared to CCSM3 (H) as is total precipitation in these regions, but in this case large-scale precipitation is reduced over much of the high latitudes and the higher total precipitation is due to convective processes. Midlatitude precipitation maxima within the ECHAM5 simulation arise from large-scale mechanisms rather than convection; however, this is also true of the preindustrial simulation and does not relate to Eocene boundary conditions.

In the warmest FAMOUS simulations of Sagoo et al. (2013), the high latitudes experience particularly significant increases in large-scale precipitation, such that the maximum values are those at the poles in the E17 simulation, and in the Southern Hemisphere the local midlatitude precipitation maximum is lost. Elevated midlatitude temperatures in the warm FAMOUS simulations additionally result in significant increases in convective precipitation which are not simulated in the cooler simulations and models. Overall, convective precipitation in FAMOUS increases as both global temperatures rise and equatorial-to-polar temperature gradients decrease, regardless of the underlying parameter configuration; this emphasises the fundamental control of temperature distribution on precipitation, as opposed to the effect of alteration of any one specific parameter.

Improvements in the simulation of precipitation in modern-day climate simulations are often related to better resolved topography (e.g. Gent et al., 2010). However, given the variety of differences in boundary conditions between the EoMIP simulations, topography appears to only have limited power in explaining differences between regional precipitation responses. Figure S5 shows differences in topography and precipitation rate between three sets of simulations with similar global precipitation rates: (i) HadCM3L and FAMOUS, where the models have similar parameterisation schemes but differ in atmospheric grid resolution; (ii) CCSM3 (W) and HadCM3L – different models, but with a similar resolution; (iii) CCSM3 (W) and CCSM3 (H) – the same model but slightly different topographic boundary conditions. The HadCM3L and CCSM3 (W) simulations show some substantial differences in the topography around the Rockies, with the increased elevation in CCSM3 possibly accounting for the increased precipitation in this region. However, differences in topography over the Asian subcontinent do not result in any systematic differences in precipitation rate. Regions of similar topography elsewhere, including over the tropics, have far more divergent precipitation responses between the models, which do not relate to local differences in topography.

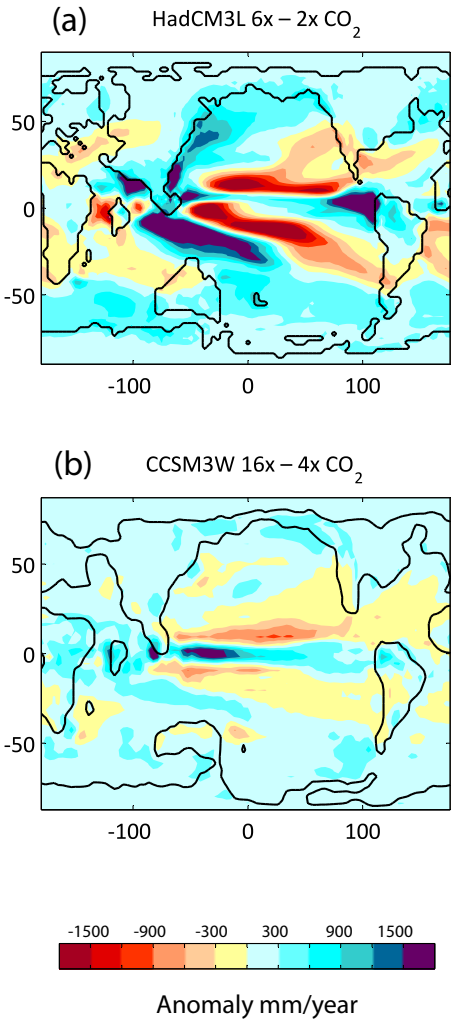

Figure 6. Anomaly plots for mean annual precipitation in millimetres per year between high and low CO_2. Eocene model simulations for **(a)** HadCM3L at x6 CO_2–x2 CO_2 and **(b)** CCSM3 (W) at x16–x4 CO_2.

For HadCM3L and CCSM3, simulations at different CO_2 concentrations provide an insight into how regional Eocene precipitation distributions are impacted by warming, and anomaly plots for high CO_2 simulations minus low CO_2 simulations are shown in Fig. 6. For the same CO_2 forcing, CCSM3 is globally cooler than HadCM3L (Lunt et al.,

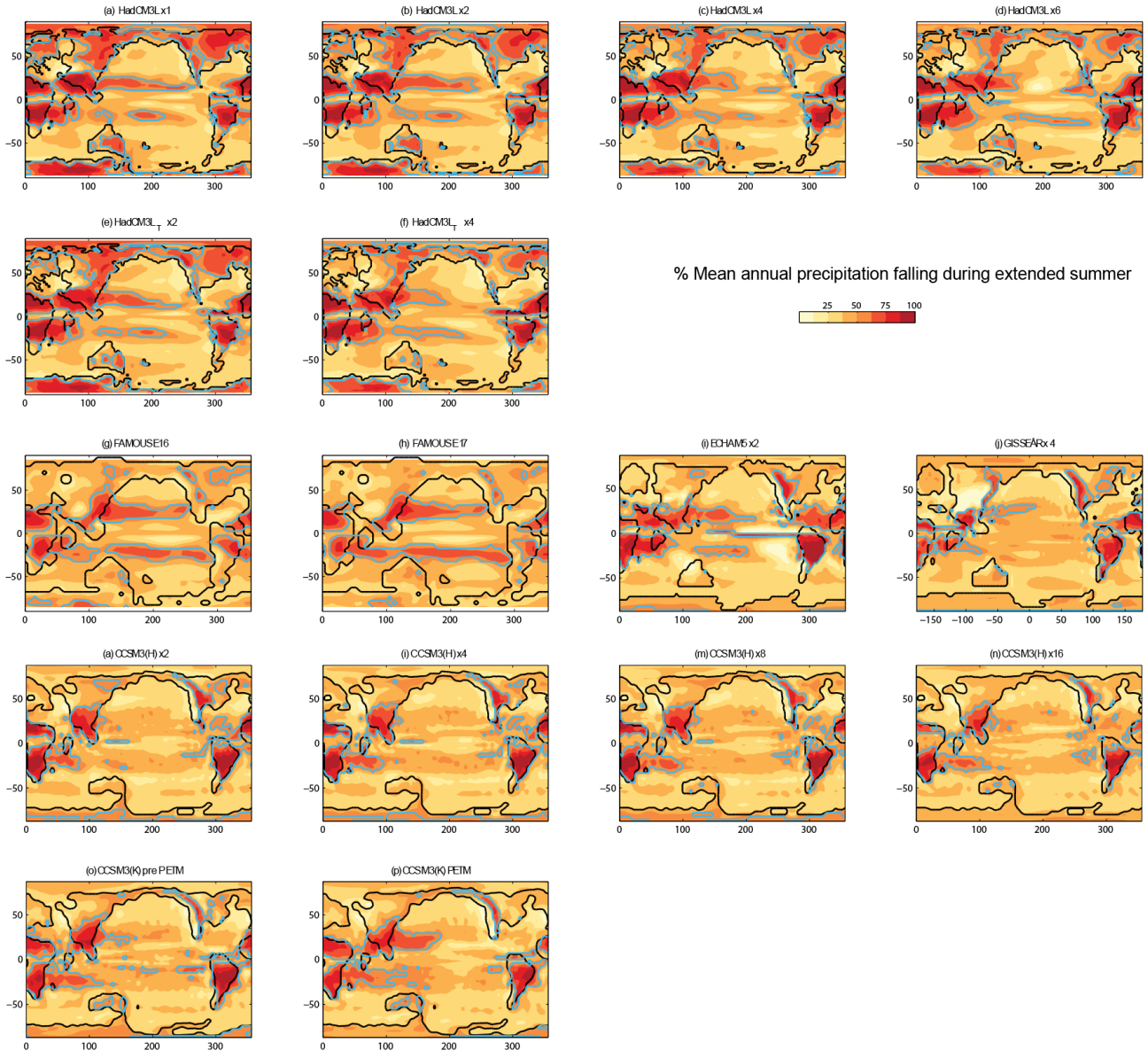

Figure 7. Percentage of mean annual precipitation falling in the extended summer season (MJJAS for Northern Hemisphere, NDJFM for Southern Hemisphere; early Eocene paleogeography); regions with > 55 % summer precipitation are outlined in blue. Results from preindustrial simulations are shown in the Supplement. CO_2 for each model simulation is shown above each plot. The FAMOUS simulations are both at x2 CO_2.

2012), but the anomalies for x16–x4 CO_2 (CCSM (W)) and x6–x2 CO_2 (HadCM3L) display similar global changes in temperature and therefore precipitation rate on account of similar dP/dT relationships (Fig. 2; Table 2). Intriguingly, HadCM3L displays far greater spatial contrasts in net precipitation change, particularly over the ocean: between the pair of HadCM3L simulations, some 23 % of the Earth's surface experiences an increase or decrease in precipitation greater than 60 cm yr^{-1}, compared to just 6 % in the CCSM3 simulations. Ignoring differences in the spatial pattern of atmospheric circulation, such as those relating to differing SPCZ (Sect. 3.3.1), the underlying response appears to be an increase in precipitation in the deep tropics and a reduction in precipitation in the subtropics, at least over the Pacific Ocean. This increase in moisture in the convergence zone and decrease in the divergence zones appears to relate to a more vigorous change in tropical atmospheric circulation in the HadCM3L model relative to CCSM3 (Fig. S6). Spatial patterns are additionally model dependent: in HadCM3L, there is a clear increase in the strength of storm tracks along the eastern Asian coastline, which is not repeated in CCSM3. In HadCM3L, decreases in precipitation occur around the Peri-

Table 3. Percentage of land surface characterised by extended summer precipitation > 55 % MAP by model and by fractionation CO_2 increase from preindustrial (PI) conditions.

Model	PI	× 1 CO_2	× 2 CO_2	× 4/5 CO_2	× 6/8/9 CO_2	× 16 CO_2
HadCM3L	60.1	66.3	62.6	57.7	52.3	
HadCM3L (T)			62.0	51.6		
ECHAM5	50.1		41.6			
GISS-ER	47.7			37.6		
CCSM3 (H)	50.1		47.3	44.2	42.4	35.1
CCSM3 (K)				47.5	34.1	
FAMOUS	48.9		28.1 E16			
			23.6 E17			

Tethys and along the coastline of equatorial Africa. Therefore, although models within the EoMIP ensemble exhibit similarities in their global rate of precipitation change with respect to temperature, regional precipitation distributions are strongly model dependent.

3.4 Precipitation seasonality

The evolution and timing of the onset of global monsoon systems in the Eocene has been the subject of debate (Licht et al., 2014; Sun and Wang, 2005; Wang et al., 2013). Proxy studies for the early Eocene have highlighted differences in precipitation seasonality relative to modern conditions (Greenwood et al., 2010; Greenwood, 1996; Schubert et al., 2012) and geochemical and sedimentological changes at the PETM have also been attributed to changes in seasonality (Sluijs et al., 2011; Schmitz and Pujalte, 2007; Handley et al., 2012). Previous modelling work utilising CCSM3 has suggested that much of the mid–late Eocene was monsoonal, with up to 70 % of annual rainfall occurring during one extended season in northern and southern Africa, North and South America, Australia, and Indo-Asia (Huber and Goldner, 2012). However, GCMs have been shown to differ greatly in their prediction of future monsoon systems (e.g. Turner and Slingo, 2009; Chen and Bordoni, 2014), and therefore we examine the similarities and differences in Eocene models with respect to the seasonality of their precipitation distributions.

Figure 7 shows the percentage of precipitation falling in the extended summer season (MJJAS for Northern Hemisphere; NDJFM for Southern Hemisphere) following the approach of Zhang and Wang (2008) also utilised in the Eocene studies of Huber and Goldner (2012) and Licht et al. (2014). This metric has been shown to correlate well with the modern-day distribution of monsoon systems. Overall, the models show a global distribution of early Eocene monsoons in high-CO_2 climates that is similar to those simulated under preindustrial simulations (Fig. S7). Australia is markedly less monsoonal than in preindustrial simulations due to its more southerly Eocene paleolocation. Note that regions where winter season precipitation dominates fall at the lower end of the scale, these tend to be over the ocean surface but also include regions around the Peri-Tethys and both the Pacific and Atlantic US coasts.

HadCM3L is notable in that it is more seasonal at high latitudes, simulating an early Eocene monsoon centred over modern-day Wilkes Land region of Antarctica. Although proxy data have suggested highly seasonal precipitation regimes for both the Arctic (Schubert et al., 2012) and Antarctic (Jacques et al., 2014) during this interval, these systems are maximised in the x2 CO_2 simulation and weaken somewhat in the simulations with elevated CO_2. This arises due to the high-temperature seasonality of Arctic and Antarctic Eocene regions in HadCM3L relative to the other models (e.g. Gasson et al., 2014). In austral winter, Antarctic temperatures are sufficiently low to suppress precipitation, whilst this constraint is lifted somewhat in the higher-CO_2 simulations, which produce more equable rainfall distribution. Crucially, the effect of elevated global warmth on the extent of Eocene monsoons is consistent across the models, with higher-CO_2 simulations associated with a decline in terrestrial areas with seasonal precipitation regimes (Table 3). HadCM3L simulates a 6 % reduction in the extent of terrestrial regions influenced by monsoonal regimes for the Eocene (HadCM3L × 1 CO_2) relative to the preindustrial simulation; this reduction appears to be related to the warmer surface temperatures and the absence of the Antarctic ice sheet.

3.5 $P - E$ distributions

The difference between precipitation and evaporation ($P - E$) is essential for understanding the wider impacts of an enhanced Eocene hydrological cycle. Over land, this parameter broadly determines how much precipitation will become soil water and surface run-off, the partitioning itself being dependent on the land surface and vegetation schemes within the models (e.g. Cox et al., 1998; Oleson et al., 2004). Over the ocean, $P - E$ drives differences in salinity which can affect the Eocene ocean circulation (Bice and Marotzke, 2001; Waddell and Moore, 2008). We show mean annual ($P - E$) budgets for each of the EoMIP simulations in Fig. 8. In warmer climates, an exacerbation of existing ($P - E$) is expected – that is, the wet become wetter and the dry drier, as the moisture fluxes associated with existing atmospheric circulations intensify (Held and Soden, 2006). Broadly, the EoMIP simulations support this paradigm for the Eocene relative to preindustrial conditions (Fig. 5). CCSM3 shows fairly minor changes in the boundaries between net precipitation and net evaporation zones at higher CO_2 (Fig. 8), although the net evaporation zones in HadCM3L do migrate polewards over the eastern Pacific and North Atlantic at high CO_2. Other dynamic changes within HadCM3L are coupled to the precipitation responses: the more meridionally orientated SPCZ results in a weaker zonally averaged Southern Hemisphere evaporative zone and the expansion of precipitation along the Asian coastline results in a more positive

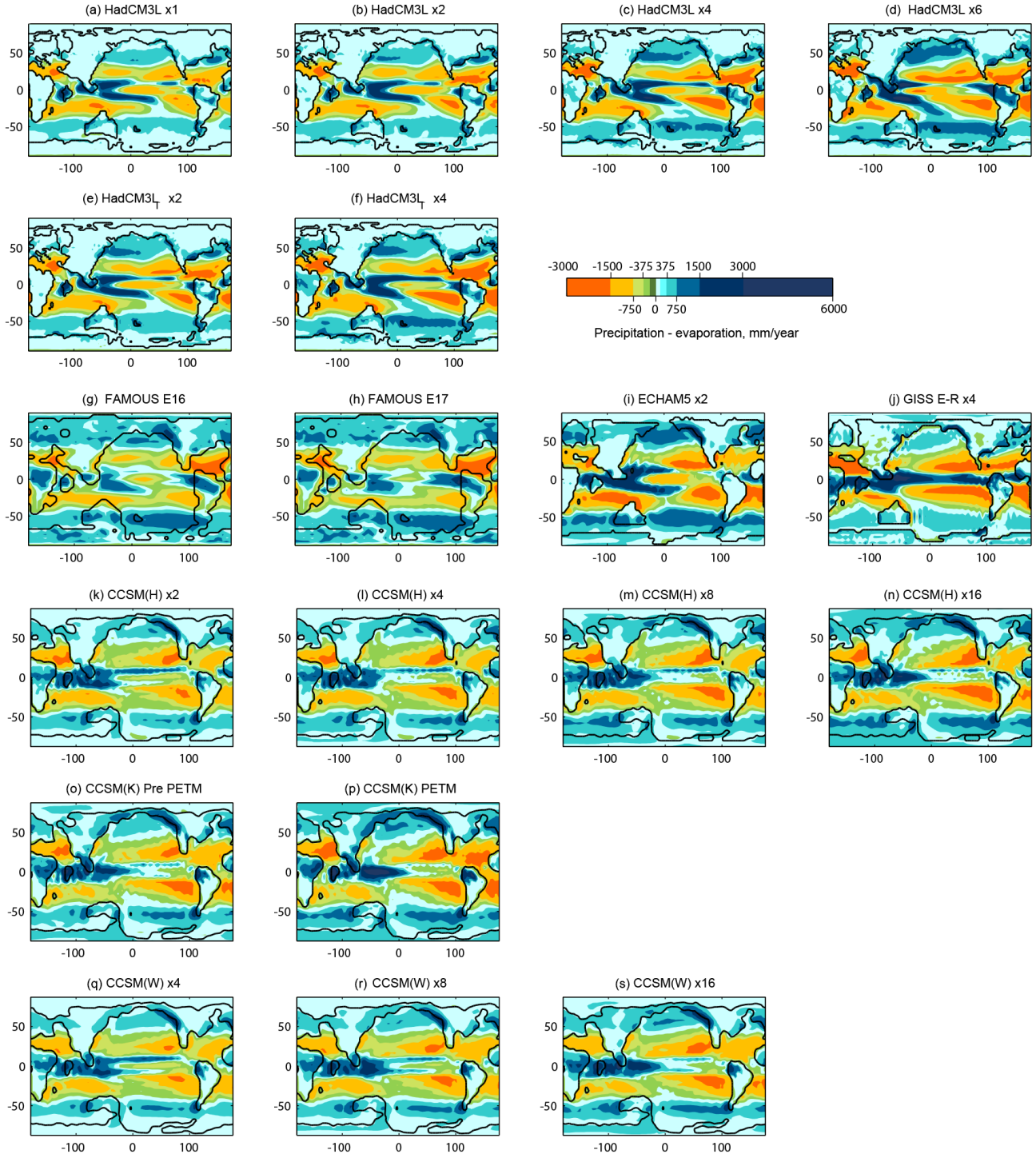

Figure 8. Mean annual $P - E$ distributions for each member of the EoMIP ensemble in millimetres per year (early Eocene paleogeography). CO_2 for each model simulation is shown above each plot. The FAMOUS simulations are both at x2 preindustrial CO_2.

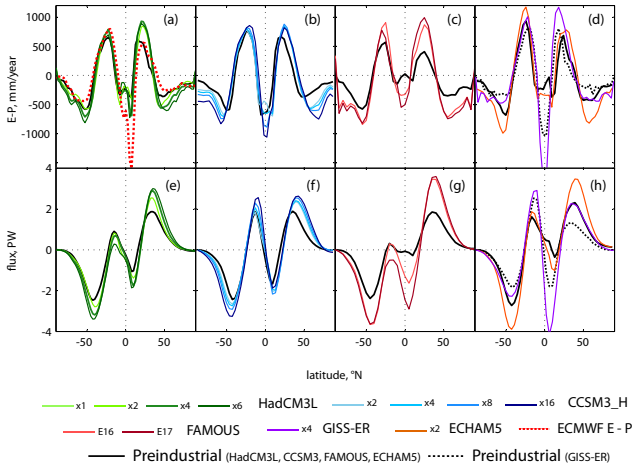

Figure 9. Latitudinal $E-P$ distributions (top) and implied northwards latent heat flux (bottom) in the EoMIP simulations. The black lines indicate preindustrial simulations, with dotted and unbroken lines in **(d, h)** corresponding to the GISS-ER and ECHAM5 simulations respectively. Heat flux expressed in petawatts (1 PW = 1015 W). Observational $E-P$ in **(a)** is based on European Centre for Medium-range Weather Forecasts (ECMWF) European Reanalysis (ERA) data (Dee et al., 2011).

($P-E$) balance in this region. Over continents the models also display different responses of $P-E$ to warming. For example, over equatorial and northern Africa, HadCM3L simulates increasingly wet climates in the high-CO_2 simulations, driven by increases in precipitation coupled to reductions in evaporation. In CCSM3, the net moisture balance is less responsive with respect to temperature, although intense equatorial precipitation means this region is much wetter than in HadCM3L.

Because of the large latent heat fluxes involved in evaporation and condensation, the global hydrological cycle acts as a meridional transport of energy. Net evaporation in the subtropics stores energy in the atmosphere as latent heat, releasing it at high latitudes via precipitation (Pierrehumbert, 2002). An intensified hydrological cycle, associated with increased atmospheric transport of water vapour, has therefore been suggested as a potential mechanism for reducing the Equator–pole temperature gradient during greenhouse climates (Ufnar et al., 2004; Caballero and Langen, 2005). By integrating the area-weighted estimates of $P-E$ with latitude, we show how these contributions differ between the EoMIP models and associated preindustrial simulations (Fig. 9). Relative to preindustrial climatology, the intensification of the hydrological cycle associated with increased drying in the net evaporative zones and increased moistening of the net precipitation zones implies a stronger latent heat flux. Within the EoMIP ensemble, the implied high poleward energy fluxes of the E16 and E17 FAMOUS simulations and x2 CO_2 ECHAM5 simulation are particularly significant. GISS-ER has a particularly strong low-latitude equatorially directed latent heat transfer which arises from the much elevated Eocene precipitation rate in the deep tropics. The asymmetry in some of the models' implied flux is due to a hemispheric imbalance in precipitation and evaporation. For example, in the FAMOUS E17 simulation, there is greater precipitation than evaporation in the Southern Hemisphere, and so more energy is released from the atmosphere by latent heat than is stored, meaning that the implied heat flux does not cross 0 at the Equator. However, since total precipitation is equal to total evaporation globally (Table S1), this is balanced out in the Northern Hemisphere; note that the intense evaporation zone over the North Atlantic is not matched in the Southern Hemisphere for this model. In the majority of the other models, there is greater symmetry in $P-E$ with latitude and the implied flux crosses close to the origin of the graph on Fig. 9.

At face value, it may seem that the elevated latent heat transport at mid- to high latitudes could contribute towards the reduced Equator–pole temperature gradient in the EoMIP simulations, but we note that theoretical and modelling-based studies suggest that increased latent heat transport is associated with an increased Equator–pole temperature gradient (Pagani et al., 2013). Within the EoMIP ensemble, meridional temperature gradients and global surface air temperatures covary, and so it is not possible to separate clearly the effects of these different controls (Fig. S8). Nevertheless, these results illustrate that relative to preindustrial conditions, the Eocene hydrological cycle acts to elevate the meridional transport of latent heat, particularly around 45–50° N and S of the Equator.

4 Proxy–model comparison

A range of proxy data provide constraints on how the early Eocene hydrological cycle differed from that of the modern day, including oxygen isotopes from mammalian, fish, and foraminiferal fossils (Clementz and Sewall, 2011; Zachos et al., 2006; Zacke et al., 2009) and from the distribution of climatically sensitive sediments (e.g. Huber and Goldner, 2012). Changes in regional hydrology at the PETM have also been inferred from geomorphological (John et al., 2008; Schmitz and Pujalte, 2007), biomarker (Handley et al., 2011; Pagani et al., 2006), and microfossil (Sluijs et al., 2011; Kender et al., 2012) proxies. These have resulted in qualitative interpretations of hydrological change, although the climatic variables and temporal signal which the proxies record are often uncertain (e.g. Handley et al., 2011, 2012; Tipple et al., 2013; Sluijs et al., 2007). However, quantitative estimates of mean annual precipitation (MAP), derived from micro- and macrofloral fossils, have been made for a number of early Eocene and PETM-aged sections, which can be compared directly with the GCM-estimated precipitation rates described in Sect. 3.

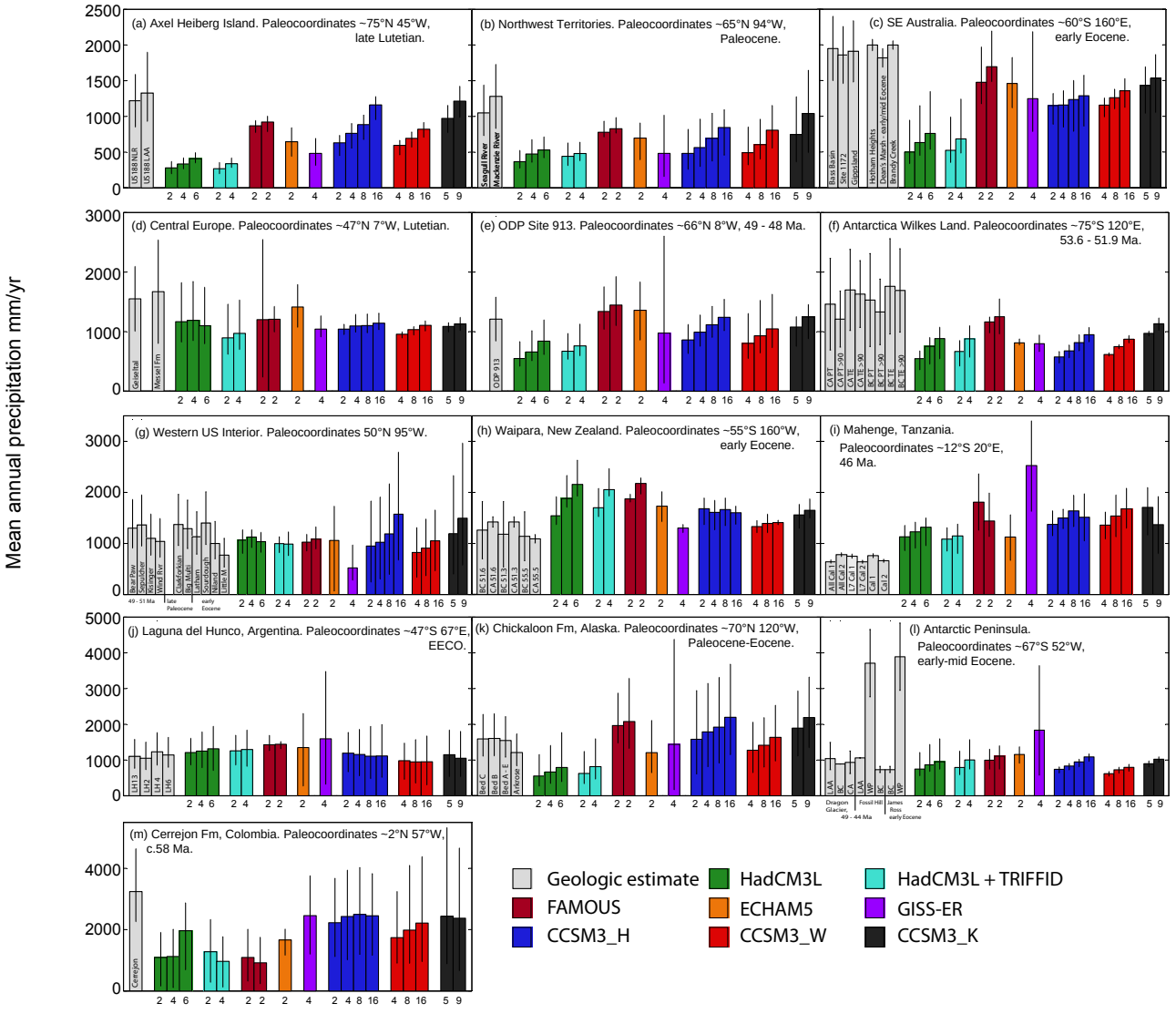

Figure 10. Proxy–model comparisons for mean annual precipitation (MAP) for the EoMIP ensemble: **(a)** Axel Heiberg Island, data from Greenwood et al. (2010); **(b)** Northwest Territories, data from Greenwood et al. (2010); **(c)** southeastern Australia and Tasmania, data from Greenwood et al. (2005) and Contreras et al. (2014); **(d)** central Europe, data from Mosbrugger et al. (2005) and Grein et al. (2011); **(e)** Ocean Drilling Program (ODP) Site 913, data from Eldrett et al. (2009); **(f)** Wilkes Land, data from Pross et al. (2012); **(g)** western US interior, data from Wilf et al. (1998) and Wilf (2000); **(h)** Waipara, New Zealand, data from Pancost et al. (2013); **(i)** Mahenge, Tanzania, data from Jacobs and Herendeen (2004) and Kaiser et al. (2006); **(j)** Argentina, data from Wilf et al. (2005); (**k**) Chickaloon Formation, Alaska, data from Sunderlin et al. (2011, 2014); **(l)** Antarctic Peninsula, data from Hunt and Poole (2003) and Poole et al. (2005); **(m)** Cerrejon Formation, data from Wing et al. (2009). Error bars show the mean with range based on nine model grid cells closest to given paleocoordinates. Full details are given in the Supplement, Table S3.

Paleoprecipitation estimates are primarily produced by two distinct paleobotanic methods: leaf physiognomy and NLR approaches. In the former, empirical univariate and multivariate relationships have been established between the size and shape of modern angiosperm leaves and the climate in which they grow, with smaller leaves predominating in low-precipitation climates (e.g. Wolfe, 1993; Wilf et al., 1998; Royer et al., 2005). The NLR approach estimates paleoclimate by assuming that fossilised specimens have the same climatic tolerances as their presumed extant relatives. This approach can utilise pollen, seeds, and fruit in addition to leaf fossils (Mosbrugger et al., 2005). Geologic estimates are less precise than mean annual air temperatures, which may relate to the decoupling between MAP and local water availability (Peppe et al., 2011; Royer et al., 2002), a greater importance of growing season climate (Mosbrugger and Utescher, 1997), or, in the case of physiognomical ap-

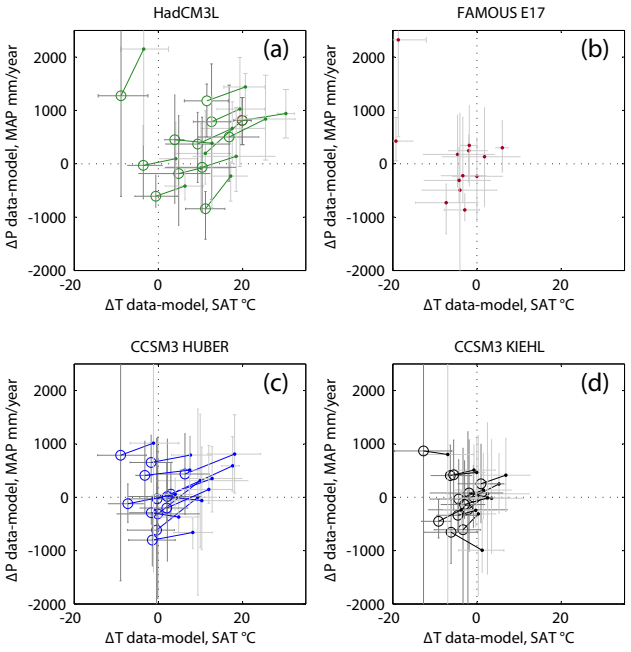

Figure 11. Surface air temperature and mean annual precipitation proxy–model anomalies for low- and high-CO_2 climates shown by closed and open circles respectively. Simulations are at x2 and x6 the CO_2 levels for HadCM3L **(a)**, E17 for FAMOUS **(b)**, x2 and x16 the CO_2 for CCSM3 (H) **(c)**, and x5 and x9 CO_2 for CCSM3 (K) **(d)**. The data points represent averaged signals for the sites shown in Fig. 10. Estimates of maximum (minimum) error are calculated as anomalies between the highest (lowest) data estimate and the lowest (highest) value within the local model grid.

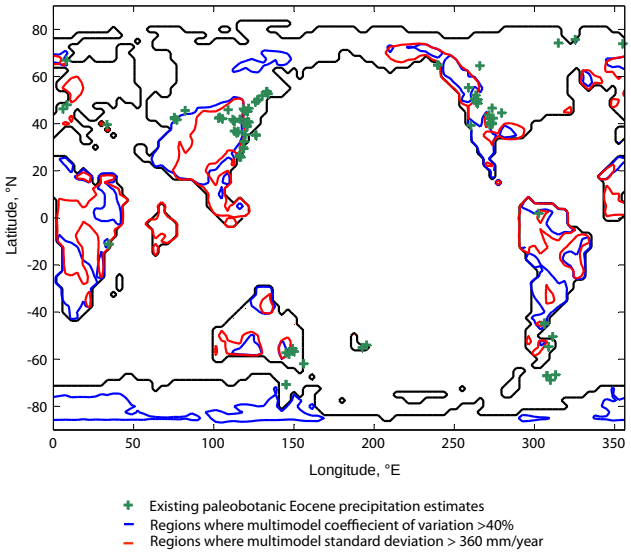

Figure 12. Summary of regions which show a significant model spread, based on the Eocene multimodel mean described in Fig. 5. Paleobotanical estimates of quantitative precipitation rate included in the data compilation are shown by green markers. Regions where the standard deviation is greater than $1\,\mathrm{mm\,day^{-1}}$ (i.e. $360\,\mathrm{mm\,yr^{-1}}$) are marked by a red outline and regions where the coefficient of variation (standard deviation / multimodel mean) is greater than 40 % are outlined blue.

proaches, competing influence of other climatic variables on leaf form (Royer et al., 2007).

Our data compilation is provided in Table S3. Some of the data has been compared previously with precipitation rates from an atmosphere-only simulation performed with isoCAM3 (isotope-enabled Community Atmosphere Model, version 3) for the Azolla interval ($\sim$ 49 Ma; Speelman et al., 2010). Our proxy–model comparison includes data for the remainder of the early–mid-Eocene, including a number of recently published estimates such that the geographic spread is widened to include estimates from Antarctica (Pross et al., 2012), Australia (Contreras et al., 2013; Greenwood et al., 2003), New Zealand (Pancost et al., 2013), South America (Wilf et al., 2005), and Europe (Eldrett et al., 2014; Mosbrugger et al., 2005; Grein et al., 2011). We select Ypresian-aged data where multiple Eocene precipitation rates exist, including estimates for the PETM (Pancost et al., 2013), but additionally include some Lutetian and Paleocene data, particularly in regions where Ypresian data do not exist. This approach is justified in some respects given the range of plausible Eocene CO_2 with which simulations have been performed. However, each data point is an independent estimate of precipitation for a given point in time, and direct comparisons between data points are hindered given that considerable climatic change occurred throughout this interval (e.g. Zachos et al., 2008; Littler et al., 2014); comparisons are particularly difficult at sites where age control is poor and the proxies could potentially reflect a range of climatic states or atmospheric CO_2 (Sect. 1).

Figure 10 shows paleobotanical estimates for MAP for a range of the data in Table S3, along with model-estimated rates for each of the EoMIP simulations. Mean precipitation estimates from each model are derived by averaging over grid boxes centred on the paleolocation in a similar approach to Speelman et al. (2010). This is a nine-cell grid of three by three grid boxes for HadCM3L, GISS-ER, ECHAM5, and CCSM3, although in some instances an eight-cell grid of two by four is used along paleocoastlines. Differing model resolutions and land–sea masks result in averaging signals from slightly different paleogeographic areas, but this approach allows for an assessment of the regional signal, and error bars are included to show the range of precipitation rates present within the locally defined grid. In the reduced-resolution model, FAMOUS, mean and range are derived from two by two grid boxes to ensure that regional climatologies remain comparable. Error bars on the geologic data are generally provided as described in the original publications, with further details also provided in Table S3.

Our results confirm different regional sensitivities across the models. For example, over New Zealand (Fig. 10b),

HadCM3L shows a strong sensitivity to increases in CO_2, whereas in CCSM3, elevated CO_2 has little effect on precipitation rate. This arises from differing SPCZ precipitation structures, with HadCM3L simulating a shift of the rain belt towards New Zealand in the warmer simulations (Fig. 6). Conversely, in the western US (Fig. 10g), HadCM3L precipitation is stable with respect to increases in CO_2 whilst CCSM3 produces increases in precipitation in higher-CO_2 simulations. Furthermore, significant variations occur between the degree of match the models show with proxy precipitation estimates. At grid boxes corresponding to modern-day Axel Heiberg Island (Fig. 10h), HadCM3L and GISS-ER are unable to produce sufficient precipitation, whereas the high-CO_2 CCSM3 and E16 and 17 FAMOUS simulations are in closer agreement. Over Wilkes Land, Antarctica, all of the EoMIP models show sensitivity to CO_2, but all produce too little precipitation, although the FAMOUS and CCSM (K) simulations with warmer polar temperatures (Fig. 4) come closest to replicating the central estimates of geologic data. However, some caution is required in how these differences are interpreted, given that preindustrial GCM errors are also typically of the order of 300 mm yr^{-1} too little precipitation over this region. A similar pattern is apparent in the Paleocene Northwest Territory data (Fig. 10l), with the models using low CO_2 and/or yielding cooler polar temperatures showing a dry bias. At the midlatitudes, model biases relative to paleoprecipitation estimates are reduced, including for the continental US (Fig. 10f), Argentina (Fig. 10g), and central Europe (Fig. 10m), where proxy data are within the precipitation range simulated across the suite of simulations.

At Tanzania (Fig. 10e), all model simulations appear to overestimate precipitation and in a number of models elevating CO_2 has relatively little impact on precipitation rate. In the HadCM3L simulations in particular, elevating CO_2 to levels required to produce a match with early Eocene high-latitude data results in considerable over-precipitation at this low-latitude site, although it should be noted that the Mahenge data are likely mid-Eocene in age and could be representative of a lower-CO_2 climate. With a scarcity of low-latitude data, this interpretation remains tentative, particularly given that a number of the models show a marginal preindustrial wet bias over tropical Africa (Fig. 1) and leaf physiognomic methods tend to result in lower precipitation estimates than those provided by other proxies (e.g. Peppe et al., 2011).

The most robust observation from our comparison is that the models produce too little precipitation at locations corresponding to Eocene high-latitude sites. This is consistent with suggestions that GCMs fail to simulate high-latitude warmth for the early Eocene. If high-latitude temperatures are too cold in the model, then the saturation vapour pressure of the atmosphere is suppressed. We demonstrate this coupling of data–model temperature and precipitation errors in Fig. 11. In HadCM3L, increasing CO_2 from x2 to x6 preindustrial levels decreases temperature and precipitation proxy–model differences at the majority of sites, resulting in a better overall match to the geologic data. In the case of CCSM3, a relatively good match with precipitation proxy estimates is achieved at both low and high CO_2, but models appear too cold at low CO_2. In FAMOUS and CCSM3 (K), parameter sets which reduce the Equator–pole temperature gradient and warm the high latitudes are able to minimise errors in both temperature and precipitation with the majority of the geologic data at low CO_2. However, in FAMOUS, E17 simulates surface air temperatures > 45 °C in Colombia, which produces a significant temperature data–model anomaly. Whilst our compilation allows for some degree of model intercomparison, it is far from a global data set, with a bias towards mid- and high-latitude sites, and a lack of data from low latitudes (Fig. 12; S9). Caution is also required in interpretation given that the data points span the early to mid-Eocene. Although few are dated to the hyperthermals (Table S3), considerable climatic change occurred throughout this dynamic interval (Sect. 1) and the data cannot be assumed to reflect a single CO_2 forcing. There is therefore a need for further proxy–model comparisons to corroborate our analysis.

An alternative explanation for the data–model mismatch is that the proxies from high latitudes are seasonally biased recorders of precipitation. The seasonality of the Canadian Arctic during the early Paleogene has been the subject of much interest, with indicators such as reptile and *Coryphodon* fossils suggesting an equable climate (e.g. Eberle et al., 2014; Eberle and Greenwood, 2012). However, recent analysis of carbon isotopes across tree rings within early–middle Eocene mummified wood has suggested that 3 times as much precipitation fell within the summer season compared to winter (Schubert et al., 2012). Given the extreme winter darkness at such latitudes (e.g. Erberle and Greenwood, 2012), it is possible that proxies are not sensitive to the annual precipitation signal but rather to a shorter, wetter growing season, especially because leaf size is thought to be a trade-off between maximising photosynthesis and minimising water loss (e.g. Peppe et al., 2011). Furthermore, the paleobotanic estimates included here support the concept of a "fossil climate" at high latitudes, i.e. a paleoclimatic state with no modern analogue, which compromises the application of the NLR concept and leaf area analysis, which are calibrated on climatic tolerances of modern-day vegetation distribution. Such an explanation is possible for the models that are cooler at the poles, such as HadCM3L, and that show a clear seasonal cycle in precipitation (Fig. 5); it is less convincing for those models that show a more equable distribution. There is, therefore, a need for further proxy studies which characterise high-latitude precipitation regimes (e.g. Jahren and Sternberg, 2008; Jahren et al., 2009; Schubert et al., 2012). Nonetheless, current best estimates of early and mid-Eocene precipitation rate provide independent evidence for a proxy–model anomaly at high latitudes.

5 Conclusions

The simulations within the EoMIP ensemble support an intensified hydrological cycle for the early Eocene, characterised by enhanced global mean precipitation and evaporation rates and increased meridional latent heat transport. The sensitivity of Eocene precipitation rates to warming is within the range suggested for future IPCC-style climate change scenarios, although some variation is introduced by models which incorporate additional feedbacks, such as the TRIFFID simulations of Loptson et al. (2014). Differences in Eocene surface temperature distributions drive differences between models in their regional precipitation rates including models with similar global precipitation sensitivities ($\mathrm{d}P/\mathrm{d}T$). Anomalies between simulations at high and low CO_2 may provide a way by which to constrain changes in precipitation that occur during hyperthermals (Winguth et al., 2010). Regions which are particularly different between HadCM3L and CCSM3 include coastal regions around the Peri-Tethys, the South Pacific, and tropical Africa, which may represent targets for future proxy-data acquisition. We additionally show a summary of where the greatest model spread in some of the simulations of the EoMIP ensemble can be found, along with the existing paleobotanic precipitation estimates in Fig. 12. This emphasises the need for additional data from the low latitudes in order to assess which models perform most realistically. There is now a need to move towards coordinated Eocene experiments between modelling groups, which will improve the ability to mechanistically explain inter-model differences. Simulations with higher-resolution "state-of-the-art" GCMs would also be valuable, given the impacts that the improved representation of orography and smaller-scale atmospheric dynamics have had in reducing biases such as double ITCZ, the representation of storm tracks, and monsoon precipitation (Hack et al., 2006; Delworth et al., 2012; Gent et al., 2010).

Our proxy comparison emphasises the coupling between temperature and precipitation data–model anomalies. For high-latitude sites, model simulations are typically too cold, resulting in suppressed precipitation across a number of the models. Model simulations which enhance high-latitude warmth are in better agreement with existing proxy data, but the size of precipitation error bars prevents the identification of a "best" simulation. Models which warm the poles via high CO_2 (Liu et al., 2009; Winguth et al., 2010) are as successful as models which achieve warmth at low CO_2 by varying poorly constrained parameter values (Sagoo et al., 2013; Kiehl and Shields, 2013). Better constraints on uncertain early Eocene boundary conditions, including CO_2, and more data from low latitudes are now required, as are other proxy approaches which can verify the high-latitude anomaly we have observed. Forward proxy modelling of water isotopes (Speelman et al., 2010; Sturm et al., 2009; Tindall et al., 2010) and a comparison to archives which incorporate an Eocene δD or $\delta^{18}O$ signal (Zacke et al., 2009; Krishnan et al., 2014; Fricke and Wing, 2004) represent one such avenue. Given the potential for paleobotanic proxies to record a growing season signal in the high latitudes, alternative approaches to reconstructing precipitation seasonality are now needed (Schubert et al., 2012).

Proxies sensitive to hydrological changes offer a method independent of temperature by which to assess paleoclimatic model performance. Whilst elevated CO_2 causes a near-global increase in model-simulated surface temperatures, the same warming results in regions of both increased and reduced precipitation and $P-E$ within climate models (Figs. 5 and 9). Even without tightly constrained absolute changes in precipitation or net hydrological balance, the spatial pattern of qualitative indicators may prove a critical test of GCM ability for warm paleoclimates. Where estimates of absolute precipitation rates do exist, our preliminary model–data comparison indicates that GCMs are broadly unable to simulate sufficient high-latitude precipitation for the early Eocene, even with CO_2 configured at the upper end of proxy-inferred estimates. Precipitation biases within models are coupled to those of temperature and our analysis is therefore consistent with the prevailing view of enhanced early Eocene high-latitude warmth. Our study represents a first step towards characterising the variability of the Eocene hydrological cycle simulated in GCMs. Further work is now required to study how other modelled aspects of the hydrological cycle such as run-off and salinity vary within the Eocene and how these hydrological changes may relate to signals preserved in the geological record.

The Supplement related to this article is available online at doi:10.5194/cp-12-455-2016-supplement.

Acknowledgements. Daniel J. Lunt acknowledges support through the NERC grant Cretaceous–Paleocene–Eocene: Exploring Climate and Climate Sensitivity (NE/K014757/1). Richard D. Pancost acknowledges the Royal Society for a Wolfson Research Merit Award. Finally, we thank two anonymous reviewers for their constructive comments, which improved the quality of this manuscript.

Edited by: G. Dickens

References

Abbot, D. S. and Tziperman, E.: A high-latitude convective cloud feedback and equable climates, Q. J. Roy. Meteor. Soc., 134, 165–185, doi:10.1002/qj.211, 2008.

Adler, R. F., Huffman, G. J., Chang, A., Ferraro, R., Xie, P., Janowiak, J., Rudolf, B., Schneider, U., Curtis, S., Bolvin, D., Gruber, A., Susskind, J., and Arkin, P.: The Version 2 Global Precipitation Climatology Project (GPCP) Monthly Precipitation Analysis (1979–Present), J. Hydrometeor., 4, 1147–1167, 2003.

Allen, M. R. and Ingram, W. J.: Constraints on future changes in climate and the hydrologic cycle, Nature, 419, 224–232, doi:10.1038/nature01092, 2002.

Beerling, D. J., Fox, A., Stevenson, D. S., and Valdes, P. J.: Enhanced chemistry climate feedbacks in past greenhouse worlds, P. Natl. Acad. Sci. USA, 108, 9770–9775, doi:10.1073/pnas.1102409108, 2011.

Bice, K. L. and Marotzke, J.: Numerical evidence against reversed thermohaline circulation in the warm Paleocene/Eocene ocean, J. Geophys. Res.-Oceans, 106, 11529–11542, doi:10.1029/2000jc000561, 2001.

Bijl, P. K., Schouten, S., Sluijs, A., Reichart, G. J., Zachos, J. C., and Brinkhuis, H.: Early Palaeogene temperature evolution of the southwest Pacific Ocean, Nature, 461, 776–779, doi:10.1038/Nature08399, 2009.

Bijl, P. K., Bendle, J. A. P., Bohaty, S. M., Pross, J., Schouten, S., Tauxe, L., Stickley, C. A., McKay, R. M., Rohl, U., Olney, M., Sluijs, A., Escutia, C., Brinkhuis, H., and Expedition 318 Scientists: Eocene cooling linked to early flow across the Tasmanian Gateway, P. Natl. Acad. Sci. USA, 110, 9645–9650, doi:10.1073/pnas.1220872110, 2013.

Bolle, M. P. and Adatte, T.: Palaeocene early Eocene climatic evolution in the Tethyan realm: clay mineral evidence, Clay Miner., 36, 249–261, doi:10.1180/000985501750177979, 2001.

Bolle, M. P., Pardo, A., Adatte, T., Tantawy, A. A., Hinrichs, K. U., Von Salis, K., and Burns, S.: Climatic evolution on the southern and northern margins of the Tethys from the Paleocene to the early Eocene, GFF, 122, 31–32, doi:10.1080/11035890001221031, 2000.

Bony, S., Bellon, G., Klocke, D., Sherwood, S., Fermepin, S., and Denvil, S.: Robust direct effect of carbon dioxide on tropical circulation and regional precipitation, Nat. Geosci., 6, 447–451, doi:10.1038/ngeo1799, 2013.

Bowen, G. J., Beerling, D. J., Koch, P. L., Zachos, J. C., and Quattlebaum, T.: A humid climate state during the Palaeocene/Eocene thermal maximum, Nature, 432, 495–499,doi:10.1038/Nature03115, 2004.

Braconnot, P., Harrison, S. P., Kageyama, M., Bartlein, P. J., Masson-Delmotte, V., Abe-Ouchi, A., Otto-Bliesner, B., and Zhao, Y.: Evaluation of climate models using palaeoclimatic data, Nature Climate Change, 2, 417–424, doi:10.1038/nclimate1456, 2012.

Brown, J. R., Power, S. B., Delage, F. P., Colman, R. A., Moise, A. F., and Murphy, B. F.: Evaluation of the South Pacific convergence zone in IPCC AR4 climate model simulations of the twentieth century, J. Climate, 24, 1565–1582, doi:10.1175/2010JCLI3942.1, 2011.

Caballero, R. and Langen, P. L.: The dynamic range of poleward energy transport in an atmospheric general circulation model, Geophys. Res. Lett., 32, L02705, doi:10.1029/2004GL021581, 2005.

Cai, W., Lengaigne, M., Borlace, S., Collins, M., Cowan, T., McPhaden, M. J., Timmermann, A., Power, S., Brown, J., Menkes, C., Ngari, A., Vincent, E. M., and Widlansky, M. J.: More extreme swings of the South Pacific convergence zone due to greenhouse warming, Nature, 488, 365–369, doi:10.1038/nature11358, 2012.

Chadwick, R., Boutle, I., and Martin, G.: Spatial Patterns of Precipitation Change in CMIP5: Why the Rich Do Not Get Richer in the Tropics, J. Climate, 26, 3803–3822, doi:10.1175/JCLI-D-12-00543.1, 2012.

Chen, J. and Bordoni, S.: Intermodel spread of East Asian summer monsoon simulations in CMIP5, Geophys. Res. Lett., 41, 1314–1321, doi:10.1002/2013GL058981, 2014.

Chou, C. and Neelin, J. D.: Mechanisms of Global Warming Impacts on Regional Tropical Precipitation, J. Climate, 17, 2688–2701. doi:10.1175/1520-0442(2004)017< 2688:MOGWIO> ,2.0.CO;2, 2014.

Chou, C., Neelin, J. D., Chen, C. A., and Tu, J. Y., Evaluating the "rich-get-richer" mechanism in tropical precipitation change under global warming, J. Climate, 22, 1982–2005, doi:10.1175/2008JCLI2471.1, 2009.

Clementz, M. T. and Sewall, J. O.: Latitudinal gradients in greenhouse seawater 18O: evidence from Eocene sirenian tooth enamel, Science, 332, 455–458, doi:10.1126/science.1201182, 2011.

Collins, M., Knutti, R., Arblaster, J., Dufresne, J.-L., Fichefet, T., Friedlingstein, P., Gao, X., Gutowski, W. J., Johns, T., Krinner, G., Shongwe, M., Tebaldi, C., Weaver, A. J., and Wehner, M: Long-term Climate Change: Projections, Commitments and Irreversibility, in: Climate Change 2013: The Physical Science Basis. Contribution of Working Group I to the Fifth Assessment Report of the Intergovernmental Panel on Climate Change, Cambridge University Press, Cambridge, UK and New York, NY, USA, doi:10.1017/CBO9781107415324.024, 1029–1136, 2013.

Collins, W. D., Bitz, C. M., Blackmon, M. L., Bonan, G. B., Bretherton, C. S., Carton, J. A., Chang, P., Doney, S. C., Hack, J. J., Henderson, T. B., Kiehl, J. T., Large, W. G., McKenna, D. S., Santer, B. D., and Smith, R. D.: The Community Climate System Model version 3 (CCSM3), J. Climate, 19, 2122–2143, doi:10.1175/JCLI-D-11-00290.1, 2006.

Contreras, L., Pross, J., Bijl, P. K., Koutsodendris, A., Raine, J. I., van de Schootbrugge, B., and Brinkhuis, H.: Early to Middle Eocene vegetation dynamics at the Wilkes Land Margin (Antarctica), Rev. Palaeobot. Palyno., 197, 119–142, doi:10.1016/j.revpalbo.2013.05.009, 2013.

Cramer, B. S.: Orbital climate forcing of d13C excursions in the late Paleocene–early Eocene (chrons C24n–C25n), Paleoceanography, 18, 1–25, doi:10.1029/2003PA000909, 2003.

Cox, P. M.: Description of the " TRIFFID " Dynamic Global Vegetation Model, Hadley Centre Technical Note, 24, 1–17, available at: http://www.metoffice.gov.uk/media/pdf/9/h/HCTN_24.pdf (last access: 16 July 2015), 2001.

Cox, P. M., Huntingford, C., and Harding, R. J.: A canopy conductance and photosynthesis model for use in a GCM land surface scheme, J. Hydrol., 212–213, 79–94, doi:10.1016/S0022-1694(98)00203-0, 1998.

Cox, P. M., Betts, R. A., Jones, C. D., Spall, S. A., and Totterdell, I. J.: Acceleration of global warming due to carbon-cycle feedbacks in a coupled climate model, Nature, 408, 184–187, doi:10.1038/35041539, 2000.

Dai, A.: Precipitation characteristics in eighteen coupled climate models, J. Climate, 19, 4605–4630, doi:10.1175/Jcli3884.1, 2006.

Dee, D. P., Uppala, S. M., Simmons, A. J., Berrisford, P., Poli, P., Kobayashi, S., Andrae, U., Balmaseda, M.A., Balsamo, G., Bauer, P., Bechtold, P., Beljaars, A.C.M., Van de Berg, L., Bidlot, J., Bormann, N., Delsol, C., Dragani, R., Fuentes, M., Geer,

A.J., Haimberger, L., Healy, S.B., Hersbach, H., Hólm, E.V., Isaksen, L., Kållberg, P., Köhler, M., Matricardi, M., Mcnally, A.P., Monge-Sanz, B.M., Morcrette, J.J., Park, B.K., Peubey, C., de Rosnay, P., Tavolato, C., Thépaut, J.N., Vitart, F.: The ERA-Interim reanalysis: Configuration and performance of the data assimilation system, Q. J. Roy. Meteor. Soc., 137, 553–597, doi:10.1002/qj.828, 2011.

Delworth, T. L., Rosati, A., Anderson, W., Adcroft, A. J., Balaji, V., Benson, R., Dixon, K., Griffies, S. M., Lee, H.-C., Pacanowski, R. C., Vecchi, G. A., Wittenberg, A. T., Zeng, F., and Zhang, R.: Simulated climate and climate change in the GFDL CM2.5 high-resolution coupled climate model, J. Climate, 25, 2755–2781, doi:10.1175/JCLI-D-11-00316.1, 2012.

Douglas, P. M. J., Affek, H. P., Ivany, L. C., Houben, A. J. P., Sijp, W. P., Sluijs, A., Schouten, S., and Pagani, M.: Pronounced zonal heterogeneity in Eocene southern high-latitude sea surface temperatures, P. Natl. Acad. Sci. USA, 111, 6582–6587, doi:10.1073/pnas.1321441111, 2014.

Dunkley Jones, T., Lunt, D. J., Schmidt, D. N., Ridgwell, A., Sluijs, A., Valdes, P. J., and Maslin, M.: Climate model and proxy data constraints on ocean warming across the Paleocene–Eocene Thermal Maximum, Earth-Sci. Rev., 125, 123–145, doi:10.1016/j.earscirev.2013.07.004, 2013.

Eberle, J. J.: A new "tapir" from Ellesmere Island, Arctic Canada – implications for northern high latitude palaeobiogeography and tapir palaeobiology, Palaeogeogr. Palaeocl., 227, 311–322, doi:10.1016/j.palaeo.2005.06.008, 2005.

Eberle, J. J. and Greenwood, D. R.: Life at the top of the greenhouse Eocene world – a review of the Eocene flora and vertebrate fauna from Canada's High Arctic, Geol. Soc. Am. Bull.,124, 3–23, doi:10.1130/B30571.1, 2012.

Eldrett, J. S., Greenwood, D. R., Harding, I. C., and Huber, M.: Increased seasonality through the Eocene to Oligocene transition in northern high latitudes, Nature, 459, 969–973, doi:10.1038/nature08069, 2009.

Eldrett, J. S., Greenwood, D. R., Polling, M., Brinkhuis, H., and Sluijs, A.: A seasonality trigger for carbon injection at the Paleocene-Eocene Thermal Maximum, Clim. Past, 10, 759–769, doi:10.5194/cp-10-759-2014, 2014.

Frakes, L. A.: Climates Throughout Geologic Time, Elsevier Scientific, Amsterdam, 310 pp., 1979.

Francis, J. E., Ashworth, A., Cantrill, D. J., Crame, J. A., Howe, J., Stephens, R., Tosolini, A.-M., and Thorn, V.: 100 million years of Antarctic climate evolution: evidence from fossil plants, in: Antarctica: a Keystone in a Changing World, Proceedings of the 10th International Symposium on Antarctic Earth Sciences, edited by: Cooper, A. K., Barrett, P. J., Stagg, H., Storey, E., Stump, E., Wise, W., and the 10th ISAES editorial team, The National Academies Press, Washington, DC, doi:10.3133/of2007-1047, 19–27, 2008.

Fricke, H. C. and Wing, S. L.: Oxygen isotope and paleobotanical estimates of temperature and 18O-latitude gradients over North America during the Early Eocene, Am. J. Sci., 304, 612–635, doi:10.2475/ajs.304.7.612, 2004.

Gasson, E., Lunt, D. J., DeConto, R., Goldner, A., Heinemann, M., Huber, M., LeGrande, A. N., Pollard, D., Sagoo, N., Siddall, M., Winguth, A., and Valdes, P. J.: Uncertainties in the modelled CO_2 threshold for Antarctic glaciation, Clim. Past, 10, 451–466, doi:10.5194/cp-10-451-2014, 2014.

Gent, P., Yeager, S., Neale, R., Levis, S., and Bailey, D.: Improvements in a half degree atmosphere/land version of the CCSM, Clim. Dynam., 34, 819–833, doi:10.1007/s00382-009-0614-8, 2010.

Greenwood, D. R.: Eocene monsoon forests in central Australia?, Aust. Syst. Bot., 9, 95–112, doi:10.1071/Sb9960095, 1996.

Greenwood, D. R., Moss, P. T., Rowett, A. I., Vadala, A. J., and Keefe, R. L.: Plant communities and climate change in southeastern Australia during the early Paleogene, in: Causes and Consequences of Globally Warm Climates in the Early Paleogene, The Geological Society of America, Inc., Boulder, CO, doi:10.1130/0-8137-2369-8.365, 365–380, 2003.

Greenwood, D. R., Archibald, S. B., Mathewes, R. W., and Moss, P. T.: Fossil biotas from the Okanagan Highlands, southern British Columbia and northeastern Washington State: climates and ecosystems across an Eocene landscape, Can. J. Earth Sci., 42, 167–185, doi:10.1139/e04-100, 2005.

Greenwood, D. R., Basinger, J. F., and Smith, R. Y.: How wet was the Arctic Eocene rain forest? Estimates of precipitation from Paleogene Arctic macrofloras, Geology, 38, 15–18, doi:10.1130/G30218.1, 2010.

Grein, M., Utescher, T., Wilde, V., and Roth-Nebelsick, A.: Reconstruction of the middle Eocene climate of Messel using palaeobotanical data, Neues Jahrb. Geol. P.-A., 260, 305–318, 2011.

Greve, P., Orlowsky, B., Mueller, B., Sheffield, J., Reichstein, M., and Seneviratne, S. I.: Global assessment of trends in wetting and drying over land, Nat. Geosci., 7, 716–721, doi:10.1038/ngeo2247, 2014.

Gruber, A., Su, X. J., Kanamitsu, M., and Schemm, J.: The comparison of two merged rain gauge-satellite precipitation datasets, B. Am. Meteorol. Soc., 81, 2631–2644, doi:10.1175/1520-0477(2000)081< 2631:Tcotmr>,2.3.Co;2, 2000.

Hack, J. J., Caron, J. M., Danabasoglu, G., Oleson, K. W., Bitz, C., and Truesdale, J. E.: CCSM–CAM3 Climate Simulation Sensitivity to Changes in Horizontal Resolution, J. Climate, 19, 2267–2289, doi:10.1175/JCLI3764.1, 2006.

Hagemann, S., Arpe, K., and Roeckner, E.: Evaluation of the hydrological cycle in the ECHAM5 model, J. Climate, 19, 3810–3827, doi:10.1175/JCLI3831.1, 2006.

Handley, L., Pearson, P. N., McMillan, I. K., and Pancost, R. D.: Large terrestrial and marine carbon and hydrogen isotope excursions in a new Paleocene/Eocene boundary section from Tanzania, Earth Planet. Sc. Lett., 275, 17–25, doi:10.1016/j.epsl.2008.07.030, 2008.

Handley, L., Crouch, E. M., and Pancost, R. D.: A New Zealand record of sea level rise and environmental change during the Paleocene–Eocene Thermal Maximum, Palaeogeogr. Palaeocl., 305, 185–200, doi:10.1016/j.palaeo.2011.03.001, 2011.

Handley, L., O'Halloran, A., Pearson, P. N., Hawkins, E., Nicholas, C. J., Schouten, S., McMillan, I. K., and Pancost, R. D.: Changes in the hydrological cycle in tropical East Africa during the Paleocene–Eocene Thermal Maximum, Palaeogeogr. Palaeocl., 329, 10–21,doi:10.1016/j.palaeo.2012.02.002, 2012.

Heinemann, M., Jungclaus, J. H., and Marotzke, J.: Warm Paleocene/Eocene climate as simulated in ECHAM5/MPI-OM, Clim. Past, 5, 785–802, doi:10.5194/cp-5-785-2009, 2009.

Held, I. M. and Soden, B. J.: Robust responses of the hydrological cycle to global warming, J. Climate, 19, 5686–5699, doi:10.1175/JCLI3990.1, 2006.

Hollis, C. J., Taylor, K. W. R., Handley, L., Pancost, R. D., Huber, M., Creech, J. B., Hines, B. R., Crouch, E. M., Morgans, H. E. G., Crampton, J. S., Gibbs, S., Pearson, P. N., and Zachos, J. C.: Early Paleogene temperature history of the Southwest Pacific Ocean: reconciling proxies and models, Earth Planet. Sc. Lett., 349, 53–66, doi:10.1016/j.epsl.2012.06.024, 2012.

Huber, M.: Climate change. A hotter greenhouse?, Science, 321, 353–354, doi:10.1126/science.1161170, 2008.

Huber, M., Brinkhuis, H., Stickley, C. E., Döös, K., Sluijs, A., Warnaar, J., Schellenberg, S. A., and Williams, G. L.: Eocene circulation of the Southern Ocean: Was Antarctica kept warm by subtropical waters?, Paleoceanography, 19, 1–12, doi:10.1029/2004PA001014, 2004.

Huber, M. and Caballero, R.: The early Eocene equable climate problem revisited, Clim. Past, 7, 603–633, doi:10.5194/cp-7-603-2011, 2011.

Huber, M. and Goldner, A.: Eocene monsoons, J. Asian Earth Sci., 44, 3–23, doi:10.1016/j.jseaes.2011.09.014, 2012.

Huber, M. and Sloan, L. C.: Heat transport, deep waters, and thermal gradients: coupled simulation of an Eocene greenhouse climate, Geophys. Res. Lett., 28, 3481–3484, doi:10.1029/2001GL012943, 2001.

Hunt, R. J. and Poole, I.: Paleogene West Antarctic climate and vegetation history in light of new data from King George Island, Geol. S. Am. S., 369, 395–412, doi:10.1130/0-8137-2369-8.395, 2003.

Inglis, G. N., Farnsworth, A., Lunt, D., Foster, G. L., Hollis, C. J., Pagani, M., Jardine, P., Pearson, P. N., Markwick, P., Galsworthy, A., Raynham, A., Taylor, K. W. R., and Pancost, R. D.: Descent towards the Icehouse: Eocene sea surface cooling inferred from GDGT distributions, Paleoceanography, 30, 1000–1020, doi:10.1002/2014PA002723, 2015.

Jacobs, B. F. and Herendeen, P. S.: Eocene dry climate and woodland vegetation in tropical Africa reconstructed from fossil leaves from northern Tanzania, Palaeogeogr. Palaeocl., 213, 115–123, doi:10.1016/j.palaeo.2004.07.007, 2004.

Jacques, F. M. B., Shi, G., Li, H., and Wang, W.: An early-middle Eocene Antarctic summer monsoon: evidence of "fossil climates", Gondwana Res., 25, 1422–1428, doi:10.1016/j.gr.2012.08.007, 2014.

Jahren, A. H. and Sternberg, L. S. L.: Annual patterns within tree rings of the Arctic middle Eocene (ca. 45 Ma): Isotopic signatures of precipitation, relative humidity, and deciduousness, Geology, 36, 99–102, doi:10.1130/G23876A.1, 2008.

Jahren, A. H., Byrne, M. C., Graham, H. V., Sternberg, L. S. L., and Summons, R. E.: The environmental water of the middle Eocene Arctic: Evidence from δD, δ^{18}O and δ^{13}C within specific compounds, Palaeogeogr. Palaeoecol., 271, 96–103, doi:10.1016/j.palaeo.2008.09.016, 2009.

Joetzjer, E., Douville, H., Delire, C., and Ciais, P.: Present-day and future Amazonian precipitation in global climate models: CMIP5 versus CMIP3, Clim. Dynam., 41, 2921–2936, doi:10.1007/s00382-012-1644-1, 2013.

John, C. M., Bohaty, S. M., Zachos, J. C., Sluijs, A., Gibbs, S., Brinkhuis, H., and Bralower, T. J.: North American continental margin records of the Paleocene–Eocene thermal maximum: implications for global carbon and hydrological cycling, Paleoceanography, 23, Pa2217, doi:10.1029/2007pa001465, 2008.

John, C. M., Banerjee, N. R., Longstaffe, F. J., Sica, C., Law, K. R., and Zachos, J. C.: Clay assemblage and oxygen isotopic constraints on the weathering response to the Paleocene–Eocene thermal maximum, east coast of North America, Geology, 40, 591–594, doi:10.1130/G32785.1, 2012.

Jones, C., Gregory, J., Thorpe, R., Cox, P., Murphy, J., Sexton, D., and Valdes, P.: Systematic optimisation and climate simulation of FAMOUS, a fast version of HadCM3, Clim. Dynam., 25, 189–204, doi:10.1007/s00382-005-0027-2, 2005.

Kaiser, T. M., Ansorge, J., Arratia, G., Bullwinkel, V., Gunnell, G. F., Herendeen, P. S., Jacobs, B., Mingram, J., Msuya, C., Musolff, A., Naumann, R., Schulz, E., and Wilke, V.: The maar lake of Mahenge (Tanzania) – unique evidence of Eocene terrestrial environments in sub-Sahara Africa, Z. Dtsch. Ges. Geowiss., 157, 411–413, 2006.

Kender, S., Stephenson, M. H., Riding, J. B., Leng, M. J., Knox, R. W. O. B., Peck, V. L., Kendrick, C. P., Ellis, M. A., Vane, C. H., and Jamieson, R.: Marine and terrestrial environmental changes in NW Europe preceding carbon release at the Paleocene–Eocene transition, Earth Planet. Sc. Lett., 353–354, 108–120, doi:10.1016/j.epsl.2012.08.011, 2012.

Kiehl, J. T. and Shields, C. A.: Sensitivity of the Palaeocene–Eocene Thermal Maximum climate to cloud properties, Philos. T. R. Soc. A, 371, 20130093, doi:10.1098/Rsta.2013.0093, 2013.

Kirk-Davidoff, D. B.: On the feedback of stratospheric clouds on polar climate, Geophys. Res. Lett., 29, 1–4, doi:10.1029/2002GL014659, 2002.

Kirtland Turner, S., Sexton, P. F., Charles, C. D., and Norris, R. D.: Persistence of carbon release events through the peak of early Eocene global warmth, Nat. Geosci., 7, 748–751, doi:10.1038/ngeo2240, 2014.

Komar, N., Zeebe, R. E., and Dickens, G. R.: Understanding long-term carbon cycle trends: The late Paleocene through the early Eocene, Paleoceanography, 28, 650–662, doi:10.1002/palo.20060, 2013.

Korty, R. L., Emanuel, K. A., and Scott, J. R.: Tropical cyclone-induced upper-ocean mixing and climate: Application to equable climates, J. Climate, 21, 638–654, doi:10.1175/2007JCLI1659.1, 2008.

Knutti, R. and Sedlacek, J.: Robustness and uncertainties in the new CMIP5 climate model projections, Nature Climate Change, 3, 369–373, doi:10.1038/Nclimate1716, 2013.

Kraus, M. J., McInerney, F. A., Wing, S. L., Secord, R., Baczynski, A. A., and Bloch, J. I.: Paleohydrologic response to continental warming during the Paleocene–Eocene Thermal Maximum, Bighorn Basin, Wyoming, Palaeogeogr. Palaeocl., 370, 196–208, doi:10.1016/j.palaeo.2012.12.008, 2013.

Krishnan, S., Pagani, M., Huber, M., and Sluijs, A.: High latitude hydrological changes during the Eocene Thermal Maximum 2, Earth Planet. Sc. Lett., 404, 167–177, doi:10.1016/j.epsl.2014.07.029, 2014.

Kump, L. R. and Pollard, D.: Amplification of Cretaceous warmth by biological cloud feedbacks, Science, 320, 195, doi:10.1126/science.1153883, 2008.

Legates, D. R. and Willmott, C. J.: Mean seasonal and spatial variability in gauge-corrected, global precipitation, Int. J. Climatol., 10, 111–127, doi:10.1002/joc.3370100202, 1990.

Licht, A., van Cappelle, M., Abels, H. A., Ladant, J.-B., Trabucho-Alexandre, J., France-Lanord, C., Donnadieu, Y., Vandenberghe,

J., Rigaudier, T., Lecuyer, C., Terry Jr, D., Adriaens, R., Boura, A., Guo, Z., Soe, A. N., Quade, J., Dupont-Nivet, G., Jaeger, J.-J., and Jaeger, J.-J.: Asian monsoons in a late Eocene greenhouse world, Nature, 513, 501–506, doi:10.1038/nature13704, 2014.

Lin, J-L. L.: The double-ITCZ problem in IPCC AR4 coupled GCMs: Ocean-atmosphere feedback analysis, J. Climate, 20, 4497–4525, doi:10.1175/JCLI4272.1, 2007.

Littler, K., Röhl, U., Westerhold, T., and Zachos, J. C.: A high-resolution benthic stable-isotope record for the South Atlantic: Implications for orbital-scale changes in Late Paleocene-Early Eocene climate and carbon cycling, Earth Planet. Sc. Lett., 401, 18–30, doi:10.1016/j.epsl.2014.05.054, 2014.

Liu, C., Allan, R. P., Brooks, M., and Milton, S.: Comparing tropical precipitation simulated by the Met Office NWP and climate models with satellite observations, J. Appl. Meteorol. Climatol., 53, 200–214, doi:10.1175/JAMC-D-13-082.1, 2014.

Liu, Z., Pagani, M., Zinniker, D., Deconto, R., Huber, M., Brinkhuis, H., Shah, S. R., Leckie, R. M., and Pearson, A.: Global cooling during the eocene-oligocene climate transition, Science, 323, 1187–1190, doi:10.1126/science.1166368, 2009.

Loptson, C. A., Lunt, D. J., and Francis, J. E.: Investigating vegetation-climate feedbacks during the early Eocene, Clim. Past, 10, 419–436, doi:10.5194/cp-10-419-2014, 2014.

Lourens, L., Sluijs, A., Kroon, D., Zachos, J. C., Thomas, E., Röhl, U., Bowles, J., and Raffi, I.: Astronomical pacing of late Palaeocene to early Eocene global warming events, Nature, 435, 1083–1087, doi:10.1038/nature03814, 2005.

Lowenstein, T. K. and Demicco, R. V.: Elevated Eocene atmospheric CO_2 and its subsequent decline, Science, 313, 1928, doi:10.1126/science.1129555, 2006.

Lunt, D. J., Valdes, P. J., Jones, T. D., Ridgwell, A., Haywood, A. M., Schmidt, D. N., Marsh, R., and Maslin, M.: CO_2-driven ocean circulation changes as an amplifier of Paleocene–Eocene Thermal Maximum hydrate destabilization, Geology, 38, 875–878, doi:10.1130/G31184.1, 2010.

Lunt, D. J., Dunkley Jones, T., Heinemann, M., Huber, M., LeGrande, A., Winguth, A., Loptson, C., Marotzke, J., Roberts, C. D., Tindall, J., Valdes, P., and Winguth, C.: A model-data comparison for a multi-model ensemble of early Eocene atmosphere-ocean simulations: EoMIP, Clim. Past, 8, 1717–1736, doi:10.5194/cp-8-1717-2012, 2012.

Lunt, D. J., Farnsworth, A., Loptson, C., Foster, G. L., Markwick, P., O'Brien, C. L., Pancost, R. D., Robinson, S. A., and Wrobel, N.: Palaeogeographic controls on climate and proxy interpretation, Clim. Past Discuss., 11, 5683–5725, doi:10.5194/cpd-11-5683-2015, 2015.

Markwick, P. J.: Fossil crocodilians as indicators of Late Cretaceous and Cenozoic climates: implications for using palaeontological data in reconstructing palaeoclimate, Palaeogeogr. Palaeocl., 137, 205–271, doi:10.1016/S0031-0182(97)00108-9, 1998.

Matthews, A. J.: A multiscale framework for the origin and variability of the South Pacific Convergence Zone, Q. J. Roy. Meteor. Soc., 138, 1165–1178, doi:10.1002/qj.1870, 2012.

McInerney, F. A. and Wing, S. L.: The Paleocene-Eocene Thermal Maximum: A Perturbation of Carbon Cycle, Climate, and Biosphere with Implications for the Future, Annu. Rev. Earth Planet. Sci., 39, 489–516, doi:10.1146/annurev-earth-040610-133431, 2011.

Mehran, A., AghaKouchak, A., and Phillips, T. J.: Evaluation of CMIP5 continental precipitation simulations relative to satellite-based gauge-adjusted observations, J. Geophys. Res., 1–17, doi:10.1002/2013JD021272, 2014.

Mosbrugger, V. and Utescher, T.: The coexistence approach – a method for quantitative reconstructions of Tertiary terrestrial palaeoclimate data using plant fossils, Palaeogeogr. Palaeocl., 134, 61–86, doi:10.1016/S0031-0182(96)00154-X, 1997.

Mosbrugger, V., Utescher, T., and Dilcher, D. L.: Cenozoic continental climatic evolution of Central Europe, P. Natl. Acad. Sci. USA, 102, 14964–14969, doi:10.1073/pnas.0505267102, 2005.

Nicolo, M. J., Dickens, G. R., Hollis, C. J., and Zachos, J. C.: Multiple early Eocene hyperthermals: Their sedimentary expression on the New Zealand continental margin and in the deep sea, Geology, 35, 699–702, doi:10.1130/G23648A.1, 2007.

Oleson, K. W., Dai, Y., Bonan, G. B., Bosilovich, M., Dickinson, R. E., Dirmeyer, P., Hoffman, F., Houser, P., Levis, S., Niu, G.-Y., Thornton, P., Vertenstein, M., Yang, Z.-L., and Zeng, X.: Technical Description of the Community Land Model (CLM), NCAR Technical Note, NCAR/TN-46, 186, Boulder, CO., doi:10.5065/D6N877R0, 2004.

Pagani, M., Pedentchouk, N., Huber, M., Sluijs, A., Schouten, S., Brinkhuis, H., Sinninghe Damsté, J. S., and Dickens, G. R.: Arctic hydrology during global warming at the Palaeocene/Eocene Thermal Maximum, Nature, 442, 671–675, doi:10.1038/Nature05043, 2006.

Pagani, M., Huber, M., and Sageman, B.: Greenhouse climates, in: Treatise on Geochemistry, 2nd edn., Elsevier Ltd. Amsterdam, 6, 281–304, doi:10.1016/B978-0-08-095975-7.01314-0, 2013.

Pancost, R. D., Taylor, K. W. R., Inglis, G. N., Kennedy, E. M., Handley, L., Hollis, C. J., Crouch, E. M., Pross, J., Huber, M., Schouten, S., Pearson, P. N., Morgans, H. E. G., and Raine, J. I.: Early Paleogene evolution of terrestrial climate in the SW Pacific, Southern New Zealand, Geochem. Geophy. Geosy., 14, 5413–5429, doi:10.1002/2013gc004935, 2013.

Pearson, P. N., van Dongen, B. E., Nicholas, C. J., Pancost, R. D., Schouten, S., Singano, J. M., and Wade, B. S.: Stable warm tropical climate through the Eocene Epoch, Geology, 35, 211–214, doi:10.1130/G23175A.1, 2007.

Peppe, D. J., Royer, D. L., Cariglino, B., Oliver, S. Y., Newman, S., Leight, E., Enikolopov, G., Fernandez-Burgos, M., Herrera, F., Adams, J.M., Correa, E., Currano, E. D., Erickson, J. M., Hinojosa, L. F., Hoganson, J. W., Iglesias, A., Jaramillo, C. A., Johnson, K. R., Jordan, G. J., Kraft, N. J. B., Lovelock, E. C., Lusk, C. H., Niinemets, Ü., Peñuelas, J., Rapson, G., Wing, S. L., and Wright, I. J.: Sensitivity of leaf size and shape to climate: global patterns and paleoclimatic applications, New Phytol., 190, 724–739, doi:10.1111/j.1469-8137.2010.03615.x, 2011.

Phillips, T. J. and Gleckler, P. J.: Evaluation of continental precipitation in 20th century climate simulations: The utility of multimodel statistics, Water Resour. Res., 42, W03202, doi:10.1029/2005WR004313, 2006.

Pierrehumbert, R. T.: The hydrologic cycle in deep-time climate problems, Nature, 419, 191–198, 2002.

Poole, I., Cantrill, D., and Utescher, T.: A multi-proxy approach to determine Antarctic terrestrial palaeoclimate during the Late Cretaceous and Early Tertiary, Palaeogeogr. Palaeocl., 222, 95–121, doi:10.1016/j.palaeo.2005.03.011, 2005.

Pross, J., Contreras, L., Bijl, P. K., Greenwood, D. R., Bohaty, S. M., Schouten, S., Bendle, J. A., Rohl, U., Tauxe, L., Raine, J. I., Huck, C. E., van de Flierdt, T., Jamieson, S. S. R., Stickley, C. E., van de Schootbrugge, B., Escutia, C., Brinkhuis, H., and IODP Expedition 318 Scientists: Persistent near-tropical warmth on the Antarctic continent during the early Eocene epoch, Nature, 488, 73–77, doi:10.1038/Nature11300, 2012.

Randall, D. A., Wood, R. A., Bony, S., Colman, R., Fichefet, T., Fyfe, J., Kattsov, V., Pitman, A., Shukla, J., Srinivasan, J., Stouffer, R. J., Sumi, A., and Taylor, K. E.: Climate models and their evaluation, in: Climate Change 2007: the Physical Science Basis. Contribution of Working Group I to the Fourth Assessment Report of the Intergovernmental Panel on Climate Change, Cambridge University Press, NY, 591–662, 2007.

Robert, C. and Kennett, J. P.: Antarctic subtropical humid episode at the Paleocene–Eocene boundary: clay-mineral evidence, Geology, 22, 211–214, doi:10.1130/0091-7613(1994)022<0211:Asheat> ,2.3.Co;2, 1994.

Roberts, C. D., LeGrande, A. N., and Tripati, A. K.: Climate sensitivity to Arctic seaway restriction during the early Paleogene, Earth Planet. Sc. Lett., 286, 576–585, doi:10.1016/j.epsl.2009.07.026, 2009.

Roeckner, E., Bäuml, G., Bonaventura, L., Brokopf, R., Esch, M., Giorgetta, M., Hagemann, S., Kirchner, I., Kornblueh, L., Rhodin, A., Schlese, U., Schulzweida, U., and Tompkins, A.: The atmospheric general circulation model ECHAM5: Part 1: Model description, Deutsches Klimarechenzentrum, 349, 1–140, available at: https://www.mpimet.mpg.de/fileadmin/publikationen/Reports/max_scirep_349.pdf (last access: 16 July 2015), 2003.

Royer, D. L., Wing, S. L., Beerling, D. J., Jolley, D.W., Koch, P. L., Hickey, L. J., and Berner, R. A.: Paleobotanical evidence for near present-day levels of atmospheric CO_2 during part of the tertiary, Science, 292, 2310–2313, doi:10.1126/science.292.5525.2310, 2001.

Royer, D. L., Wilf, P., Janesko, D. A., Kowalski, E. A., and Dilcher, D. L.: Correlations of climate and plant ecology to leaf size and shape: potential proxies for the fossil record, Am. J. Bot., 92, 1141–1151, doi:10.3732/ajb.92.7.1141, 2005.

Royer, D. L., Sack, L., Wilf, P., Lusk, C. H., Jordan, G. J., Niinemets, Ü., Wright, I. J., Westoby, M., Cariglino, B., Coley, P. D., Cutter, A. D., Johnson, K. R., Labandeira, C. C., Moles, A. T., Palmer, M. B., and Valladares, F.: Fossil leaf economics quantified: calibration, Eocene case study, and implications, Paleobiology, 33, 574–589, doi:10.1666/07001.1, 2007.

Sagoo, N., Valdes, P., Flecker, R., and Gregoire, L. J.: The Early Eocene equable climate problem: can perturbations of climate model parameters identify possible solutions?, Philos. T. R. Soc. A, 371, 20130123, doi:10.1098/Rsta.2013.0123, 2013.

Schmidt, G. A., Ruedy, R., Hansen, J. E., Aleinov, I., Bell, N., Bauer, M., Bauer, S., Cairns, B., Canuto, V., Cheng, Y., Del Genio, A., Faluvegi, G., Friend, A. D., Hall, T. M., Hu, Y., Kelley, M., Kiang, N. Y., Koch, D., Lacis, A. A., Lerner, J., Lo, K. K., Miller, R. L., Nazarenko, L., Oinas, V., Perlwitz, J., Perlwitz, J., Rind, D., Romanou, A., Russell, G. L., Sato, M., Shindell, D. T., Stone, P. H., Sun, S., Tausnev, N., Thresher, D., and Yao, M. S.: Present-day atmospheric simulations using GISS ModelE: comparison to in situ, satellite, and reanalysis data, J. Climate, 19, 153–192, doi:10.1175/JCLI3612.1, 2006.

Schmitz, B. and Pujalte, V.: Abrupt increase in seasonal extreme precipitation at the Paleocene–Eocene boundary, Geology, 35, 215–218, doi:10.1130/G23261A.1, 2007.

Schubert, B. A., Jahren, A. H., Eberle, J. J., Sternberg, L. S. L., and Eberth, D. A.: A summertime rainy season in the Arctic forests of the Eocene, Geology, 40, 523–526, doi:10.1130/G32856.1, 2012.

Sewall, J. O., Sloan, L. C., Huber, M., and Wing, S.: Climate sensitivity to changes in land surface characteristics, Global Planet. Change, 26, 445–465, doi:10.1016/S0921-8181(00)00056-4, 2000.

Shellito, C. J. and Sloan, L. C.: Reconstructing a lost Eocene Paradise, Part II: On the utility of dynamic global vegetation models in pre-Quaternary climate studies, Global Planet. Change, 50, 18–32, doi:10.1016/j.gloplacha.2005.08.002, 2006.

Shellito, C. J., Lamarque, J. F., and Sloan, L. C.: Early Eocene Arctic climate sensitivity to pCO_2 and basin geography, Geophys. Res. Lett., 36, L09707, doi:10.1029/2009gl037248, 2009.

Sloan, L. C., Walker, J. C., Moore, T. C., Rea, D. K., and Zachos, J. C.: Possible methane induced polar warming in the early Eocene, Nature, 357, 320–322, doi:10.1038/357320a0, 1992.

Slotnick, B. S., Dickens, G. R., Nicolo, M. J., Hollis, C. J., Crampton, J. S., Zachos, J. C., and Sluijs, A.: Large-Amplitude Variations in Carbon Cycling and Terrestrial Weathering during the Latest Paleocene and Earliest Eocene: The Record at Mead Stream, New Zealand, J. Geol., 120, 487–505, doi:10.1086/666743, 2012.

Sluijs, A., Schouten, S., Pagani, M., Woltering, M., Brinkhuis, H., Damste, J. S. S., Dickens, G. R., Huber, M., Reichart, G. J., Stein, R., Matthiessen, J., Lourens, L. J., Pedentchouk, N., Backman, J., Moran, K., and Expedition 302 Scientists: Subtropical arctic ocean temperatures during the Palaeocene/Eocene thermal maximum, Nature, 441, 610–613, doi:10.1038/Nature04668, 2006.

Sluijs, A., Bowen, G. J., Brinkhuis, H., Lourens, L. J., and Thomas, E.: The Palaeocene-Eocene Thermal Maximum super greenhouse: biotic and geochemical signatures, age models and mechanisms of global change, in: Deep-Time Perspectives on Climate Change: Marrying the Signal from Computer Models and Biological Proxies, edited by: Williams, M., Haywood, A. M., Gregory, F. J., and Schmidt, D. N., The Geological Society, Bath, 323–350, 2007.

Sluijs, A., Schouten, S., Donders, T. H., Schoon, P. L., Röhl, U., Reichart, G., Sangiorgi, F., Kim, J-H., and Damsté, J. S. S.: Warm and wet conditions in the Arctic region during Eocene Thermal Maximum 2, Nat. Geosci., 2, 777–780, doi:10.1038/NGEO668, 2009.

Sluijs, A., Bijl, P. K., Schouten, S., Rohl, U., Reichart, G. J., and Brinkhuis, H.: Southern ocean warming, sea level and hydrological change during the Paleocene-Eocene thermal maximum, Clim. Past, 7, 47–61, doi:10.5194/Cp-7-47-2011, 2011.

Smith, F., Wing, S., and Freeman, K.: Magnitude of the carbon isotope excursion at the Paleocene–Eocene thermal maximum: the role of plant community change, Earth Planet. Sc. Lett., 262, 50–65, doi:10.1016/j.epsl.2007.07.021, 2007.

Smith, R. S. and Gregory, J.: The last glacial cycle: transient simulations with an AOGCM, Clim. Dynam., 38, 1545–1559, doi:10.1007/s00382-011-1283-y, 2012.

Smith, R. S., Gregory, J. M., and Osprey, A.: A description of the FAMOUS (version XDBUA) climate model and control

run, Geosci. Model Dev., 1, 53–68, doi:10.5194/gmd-1-53-2008, 2008.

Smith, R. Y., Greenwood, D. R., and Basinger, J. F.: Estimating paleoatmospheric pCO_2 during the Early Eocene Climatic Optimum from stomatal frequency of Ginkgo, Okanagan Highlands, British Columbia, Canada, Palaeogeogr. Palaeocl., 293, 120–131, doi:10.1016/j.palaeo.2010.05.006, 2010.

Speelman, E. N., Sewall, J. O., Noone, D., Huber, M., von der Heydt, A., Damste, J. S., and Reichart, G. J.: Modeling the influence of a reduced equator-to-pole sea surface temperature gradient on the distribution of water isotopes in the Early/Middle Eocene, Earth Planet. Sc. Lett., 298, 57–65, doi:10.1016/j.epsl.2010.07.026, 2010.

Stap, L., Lourens, L. J., Thomas, E., Sluijs, A., Bohaty, S., and Zachos, J. C.: High-resolution deep-sea carbon and oxygen isotope records of Eocene Thermal Maximum 2 and H_2, Geology, 38, 607–610, doi:10.1130/G30777.1, 2010.

Sturm, C., Zhang, Q., and Noone, D.: An introduction to stable water isotopes in climate models: benefits of forward proxy modelling for paleoclimatology, Clim. Past, 6, 115–129, doi:10.5194/cp-6-115-2010, 2010.

Suarez, M. B., Gonzalez, L. A., Ludvigson, G. A., Vega, F. J., and Alvarado-Ortega, J.: Isotopic composition of low-latitude paleoprecipitation during the Early Cretaceous, Geol. Soc. Am. Bull., 121, 1584–1595, doi:10.1130/B26453.1, 2009.

Sun, X. and Wang, P.: How old is the Asian monsoon system? – Palaeobotanical records from China, Palaeogeogr. Palaeocl., 222, 181–222, doi:10.1016/j.palaeo.2005.03.005, 2005.

Sunderlin, D., Loope, G., Parker, N. E., and Williams, C. J.: Paleoclimatic and paleoecological implications of a Paleocene–Eocene fossil leaf assemblage, Chickaloon Formation, Alaska, Palaios, 26, 335–345, doi:10.2110/palo.2010.p10-077r, 2011.

Sunderlin, D., Trop, J. M., Idleman, B. D., Brannick, A., White, J. G., and Grande, L.: Paleoenvironment and paleoecology of a Late Paleocene high-latitude terrestrial succession, Arkose Ridge Formation at Box Canyon, southern Talkeetna Mountains, Alaska, Palaeogeogr. Palaeocl., 401, 57–80, doi:10.1016/j.palaeo.2014.02.012, 2014.

Taylor, K. E., Stouffer, R. J., and Meehl, G. A.: An overview of CMIP5 and the experiment design, B. Am. Meteorol. Soc., 93, 485–498, doi:10.1175/BAMS-D-11-00094.1, 2012.

Taylor, K. W. R., Huber, M., Hollis, C. J., Hernandez-Sanchez, M. T., and Pancost, R. D.: Reevaluating modern and Palaeogene GDGT distributions: implications for SST reconstructions, Global Planet. Change, 108, 158–174, doi:10.1016/j.gloplacha.2013.06.011, 2013.

Tindall, J., Flecker, R., Valdes, P., Schmidt, D. N., Markwick, P., and Harris, J.: Modelling the oxygen isotope distribution of ancient seawater using a coupled ocean–atmosphere GCM: implications for reconstructing early Eocene climate, Earth Planet. Sc. Lett., 292, 265–273, doi:10.1016/j.epsl.2009.12.049, 2010.

Tipple, B. J., Berke, M. A., Doman, C. E., Khachaturyan, S., and Ehleringer, J. R.: Leaf-wax n-alkanes record the plant–water environment at leaf flush, P. Natl. Acad. Sci. USA, 110, 2659–2664, doi:10.1073/pnas.1213875110, 2013.

Trenberth, K. E.: Changes in precipitation with climate change, Clim. Res., 47, 123–138, doi:10.3354/cr00953, 2011.

Turner, A. G. and Slingo, J. M.: Uncertainties in future projections of extreme precipitation in the Indian monsoon region, Atmos. Sci. Lett., 10, 152–158, doi:10.1002/asl.223, 2009.

Uhl, D., Traiser, C., Griesser, U., and Denk, T.: Fossil leaves as palaeoclimate proxies in the Palaeogene of Spitsbergen (Svalbard), Acta Palaeobotanica, 47, 89–107, 2007.

Ufnar, D. F., González, L. A., Ludvigson, G. A., Brenner, R. L., and Witzke, B. J: Evidence for increased latent heat transport during the Cretaceous (Albian) greenhouse warming, Geology, 32, 1049–1052, doi:10.1130/G20828.1, 2004.

Valdes, P.: Built for stability, Nat. Geosci., 4, 414–416, doi:10.1038/ngeo1200, 2011.

Waddell, L. M. and Moore, T. C.: Salinity of the Eocene Arctic Ocean from oxygen isotope analysis of fish bone carbonate, Paleoceanography, 23, PA1S12, doi:10.1029/2007PA001451, 2008.

Wang, D., Lu, S., Han, S., Sun, X., and Quan, C.: Eocene prevalence of monsoon-like climate over eastern China reflected by hydrological dynamics, J. Asian Earth Sci., 62, 776–787, doi:10.1016/j.jseaes.2012.11.032, 2013.

White, T., Gonzalez, L., Ludvigson, G., and Poulsen, C.: Middle Cretaceous greenhouse hydrologic cycle of North America, Geology, 29, 363–366, doi:10.1130/0091-7613(2001)029< 0363:Mcghco> ,2.0.Co;2, 2001.

Wilf, P.: Late Paleocene–Early Eocene climate changes in southwestern Wyoming: paleobotanical analysis, Geol. Soc. Am. Bull., 112, 292–307, doi:10.1130/0016-7606(2000)112< 0292:Lpeecc> ,2.3.Co;2, 2000.

Wilf, P., Wing, S. L., Greenwood, D. R., and Greenwood, C. L.: Using fossil leaves as paleoprecipitation indicators: an Eocene example, Geology, 26, 203–206, doi:10.1130/0091-7613(1998)026< 0203:UFLAPI> , 2.3.Co;2, 1998.

Wilf, P., Johnson, K. R., Cuneo, N. R., Smith, M. E., Singer, B. S., and Gandolfo, M. A.: Eocene plant diversity at Laguna del Hunco and Rio Pichileufu, Patagonia, Argentina, Am. Nat., 165, 634–650, doi:10.1086/430055, 2005.

Williams, J. H. T., Smith, R. S., Valdes, P. J., Booth, B. B. B., and Osprey, A.: Optimising the FAMOUS climate model: inclusion of global carbon cycling, Geosci. Model Dev., 6, 141-160, doi:10.5194/gmd-6-141-2013, 2013.

Wing, S. L., Harrington, G. J., Smith, F. A., Bloch, J. I., Boyer, D. M., and Freeman, K. H.: Transient floral change and rapid global warming at the Paleocene–Eocene boundary, Science, 310, 993–996, doi:10.1126/science.1116913, 2005.

Wing, S. L., Herrera, F., Jaramillo, C. A., Gómez-Navarro, C., Wilf, P., and Labandeira, C. C.: Late Paleocene fossils from the Cerrejon Formation, Colombia, are the earliest record of Neotropical rainforest, P. Natl. Acad. Sci. USA, 106, 18627–18632, doi:10.1073/pnas.0905130106, 2009.

Winguth, A., Shellito, C., Shields, C., and Winguth, C.: Climate response at the Paleocene–Eocene Thermal Maximum to greenhouse gas forcing – a model study with CCSM3, J. Climate, 23, 2562–2584, doi:10.1175/2009jcli3113.1, 2010.

Winguth, A. M. E., Thomas, E., and Winguth, C.: Global decline in ocean ventilation, oxygenation, and productivity during the Paleocene–Eocene Thermal Maximum: implications for the benthic extinction, Geology, 40, 263–266, doi:10.1130/G32529.1, 2012.

Wolfe, J. A.: A method of obtaining climatic parameters from leaf assemblages, US Geological Survey Bulletin, United States Government Printing Office, Washington, 2040, 1–71, 1993.

Yapp, C. J.: Fe(CO3)OH in goethite from a mid-latitude North American Oxisol: estimate of atmospheric CO_2 concentration in the Early Eocene "climatic optimum", Geochim. Cosmochim. Ac., 68, 935–947, doi:10.1016/j.gca.2003.09.002, 2004.

Yin, L., Fu, R., Shevliakova, E., and Dickinson, R. E.: How well can CMIP5 simulate precipitation and its controlling processes over tropical South America?, Clim. Dynam., 41, 3127–3143, doi:10.1007/s00382-012-1582-y, 2013.

Yin, X., Gruber, A., and Arkin, P.: Comparison of the GPCP and CMAP merged gauge–satellite monthly precipitation products for the period 1979–2001, J. Hydrometeorol., 5, 1207–1222, doi:10.1175/JHM-392.1, 2004.

Zachos, J. C., Schouten, S., Bohaty, S., Quattlebaum, T., Sluijs, A., Brinkhuis, H., Gibbs, S. J., and Bralower, T. J.: Extreme warming of mid-latitude coastal ocean during the Paleocene–Eocene Thermal Maximum: inferences from TEX86 and isotope data, Geology, 34, 737–740, doi:10.1130/G22522.1, 2006.

Zachos, J. C., Dickens, G. R., and Zeebe, R. E.: An early Cenozoic perspective on greenhouse warming and carbon-cycle dynamics, Nature, 451, 279–283, 2008.

Zacke, A., Voigt, S., Joachimski, M. M., Gale, A. S., Ward, D. J., and Tutken, T.: Surface-water freshening and high-latitude river discharge in the Eocene North Sea, J. Geol. Soc. London, 166, 969–980, doi:10.1144/0016-76492008-068, 2009.

Zhang, S. and Wang, B.: Global summer monsoon rainy seasons, Int. J. Climatol., 28, 1563–1578, doi:10.1002/joc.1659, 2008.